Understanding SiOC Atomic Structures via Synchrotron X-ray and Reactive Force Field Potential Studies

Harrison Chaney, Yue Zhou, Kathy Lu*

Highlights:

- High energy XRD and radial distribution function analysis were used to study SiOC.
- ReaxFF provided understanding to cluster evolution and atomic radial coordination.
- Orthorhombic SiO_2 formed and converted to growth-resistant amorphous SiO_2.
- Cubic β-SiC formed at lower than reported temperatures with minor hexagonal SiC.
- ReaxFF simulation directly illustrated atomic mixing and separation.

Graphical Abstract

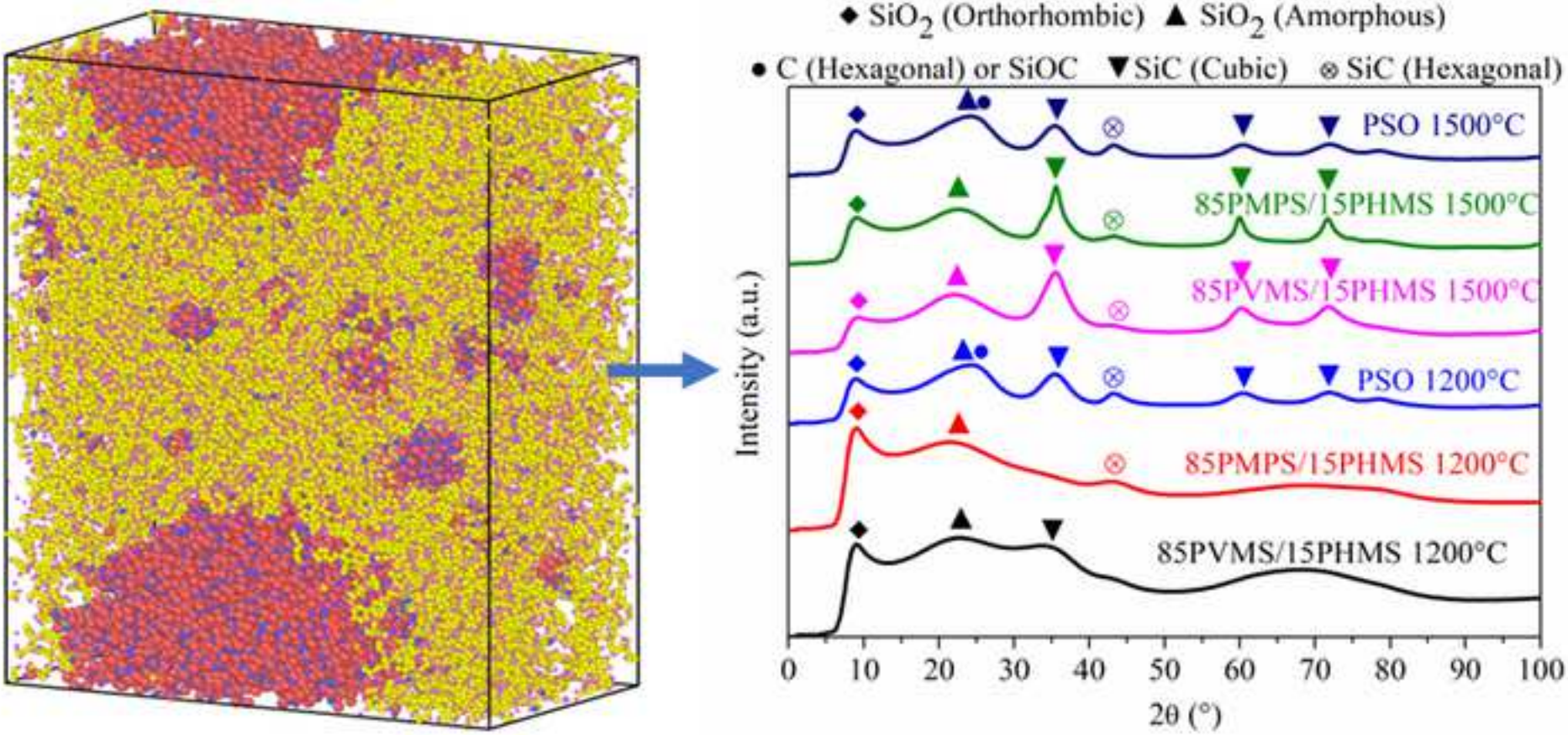

Understanding SiOC Atomic Structures via Synchrotron X-ray and Reactive Force Field Potential Studies

Harrison Chaney, Yue Zhou, Kathy Lu*

Department of Materials Science and Engineering, Virginia Polytechnic Institute and State University, Blacksburg, Virginia, 24061, USA

*Corresponding author: Email: klu@vt.edu

Declarations of interest: none

Abstract

Silicon oxycarbide (SiOC) is a unique system that can generate various compositions and microstructures via different polymeric precursors and pyrolysis conditions. However, understanding of the atomic structure evolution, such as cluster formation, phase evolution, and atomic coordination, is lacking. In this study, cluster evolution and atomic coordination for different SiOC ceramics pyrolyzed at 1200°C and 1500°C were investigated by high energy X-ray diffraction (HE-XRD) and radial distribution function (RDF) analysis. A new Reactive Force Field (ReaxFF) molecular dynamics modeling approach was developed to understand nanocluster separation and early-stage atomic radial coordination. For the first time, we demonstrate that orthorhombic SiO_2 forms and converts to growth resistant amorphous SiO_2. Cubic β-SiC also forms at lower temperatures than reported, along with a minor amount of hexagonal SiC that has never been reported. The RDF data support such phase evolution understanding. ReaxFF simulation provides direct data on atomic mixing, elemental separation, and effects of precursor molecular structures and compositions, especially in the early stage of the pyrolysis. The simulated RDF data complement the experimental data, revealing the significant presence of C-H bonds along with Si-O and C-C bonds.

Keywords: Silicon oxycarbide; High-energy X-ray diffraction; Radial distribution function; ReaxFF; Atomic structure

1. Introduction

In recent years, polymer-derived ceramics (PDCs) have attracted much attention due to their wide application potentials in energy [1, 2], environmental barrier coatings [3, 4], MEMS/NEMS devices [5, 6], biomedical engineering [7, 8], and electromagnetic interference shielding [9, 10]. Compared to conventional ceramics made by powder sintering, PDCs synthesized from polymeric precursors permit lower processing temperatures and offer great flexibility in controlling component sizes, shapes, and compositions [11, 12]. One outstanding class of PDCs is silicon oxycarbide (SiOC), an intriguing system with a three-dimensional covalently bonded structure consisting of silicon, oxygen, and carbon [13-15].

The ceramization of the most common precursor, polysiloxane, in a non-oxidizing atmosphere results in the formation of SiOC ceramics, and their compositions are determined by the pyrolysis temperature [16], atmosphere [17-21], and heating method [15, 22, 23]. Broadly speaking, a variety of C-H, Si-C, and Si-O bonds cleave at less than 1000°C and lead to the formation of free carbon dispersed in an amorphous SiOC matrix. When the temperature increases to 1100°C, the system is composed of amorphous SiOC clusters, free carbon, and amorphous SiO_2, which experience further microstructural evolution at higher pyrolysis temperatures and lead to the formation of nanocrystalline SiC, presumably at ≥1300°C [24]. Extensive work has been carried out to study the atomic structures of SiOC, such as by X-ray scattering and nuclear magnetic resonance (NMR) [25-27]. All the studies agree that SiOC materials contain SiC_xO_{4-x}

tetrahedra along with carbon domains, further supported by ^{13}C and ^{29}Si NMR measurements [28]. However, many studies also claim SiOC phase separation [15, 22, 29, 30] even though detailed atomic structure and phase evolution of SiOC materials remain evasive. Conventional structural characterization techniques cannot distinguish nanosized phases, atomic level clustering, and atomic coordination. Excitingly, HE-XRD experiments using a synchrotron light source offer improved sensitivity and resolution of diffraction peaks because of the high flux, tunable, and well-defined wavelength, as well as better collimation of synchrotron radiation [31]. This approach has great potential in clarifying the structural evolution of SiOC materials and obtaining new insights into the phase evolution of different nanoclusters within these materials. It can also offer atomic level radial distribution insight.

From modeling point of view, density functional theory and molecular dynamics approaches [32-35] have been used to provide the atomic structure of a precursor-derived amorphous ceramic. However, the simulated system sizes were inconsistent with the actual sizes of the phases, and the effects of chemical compositions on the evolution of these nano-sized structures need to be understood. Among several empirical potentials available for molecular dynamics (MD) simulations of covalent materials, the Tersoff potential provides a description of the crystalline and amorphous phases [36-39]. The total energy E of a system is expressed in terms of summation of atomic pair interactions V_{ij} between atoms i and j

$$E = \frac{1}{2}\sum_{i \neq j} V_{ij} \text{ where } V_{ij} = f_C(r_{ij})[f_R(r_{ij}) + b_{ij} f_A(r_{ij})] \quad (1)$$

r_{ij} is the distance from atom i to atom j. V_{ij} is composed of a repulsive part f_R and an attractive part f_A, and f_c is a smooth cutoff function to limit the range of the potential. However, for the polymer-derived pyrolysis process, such an interatomic potential is too simplistic [36-39]. There are several interatomic forces that have not been considered. For example, Zhang et al. [40] investigated the

structural features of an amorphous SiBOC ceramic by large-scale molecular dynamics (MD) calculations using the Tersoff potential, which uses a short-range pair potential to represent covalent bonding. Compared to the Tersoff potential which only considers the angular location of neighbor atoms relative to the bond axis, the ReaxFF potential [41] is more suitable for the simulation of PDCs, thanks to the consideration of a range of additional chemical bonding features, such as hydrogen bonding and bond conjugation. It is an empirical force field that allows for fully reactive atomistic scale molecular dynamics simulations of chemical reactions [42, 43]:

$$E_{\text{system}} = E_{\text{bond}} + E_{\text{over-coordination}} + E_{\text{under coordination}} + E_{\text{valence angle}} + E_{\text{penalty}} + E_{\text{torsion}} + E_{\text{conjugated energy}} + E_{\text{vdWaals}} + E_{\text{Coulomb}} \quad (2)$$

The energy potential functions associated with each of these partial energy contributions are developed by fitting against a training set comprised of both quantum mechanics (QM) and experimental data. This force field can simulate Si–C–O and Si–O–H bond interactions [44] and consider both reaction energies and reaction barriers. It allows evaluation of precursor effects on the elemental compositions, and more importantly, the phase distributions of the resulting SiOC systems. Furthermore, the ReaxFF method is several orders of magnitude faster than QM-based simulations, which enables larger-scale ($\gg$1000 atoms), fully dynamic simulations of chemical reactions [42, 43]. Thus, the ReaxFF potential approach is perceived to be more suitable for describing the tetrahedral structure of SiOC systems.

From simulation technique point of view, there has been simulation of PDCs from a bottom-up approach [45, 46], which involves the creation of the starting polymer structures. Afterwards, the system is heated and allowed to stay at highly elevated temperatures between 1800 and 2500 K where Si-C bond breakage is readily observable [47]. The pressures in the systems are kept high or the volumes are constrained to prevent the system from expanding continuously.

While the simulation is running, scripts are run periodically to selectively delete atoms belonging to smaller molecules such as methane and ethene groups (evaporative gases). However, such simulations have been carried out with relatively small systems of less than 80,000 starting atoms [40]. A more recent study with the ReaxFF approach reported amorphous end structures with comparable compositions to experiments. There was distinct phase separation between the carbon and SiOC phases [46]. Regardless, more systematic simulation work is needed in order to understand atomic structural unit evolution, radial distribution function, and bonding of different structural units.

In this study, synchrotron HE-XRD was used to explore the atomic structures and phase evolution of SiOC ceramics as a function of carbon content and pyrolysis temperature. Large-scale ReaxFF simulations were conducted to investigate the amorphous plus nanocluster structures of SiOC with different carbon content. The results from the experiments and the simulations were compared to understand the fundamental processes of the phase evolution and atomic bonding differences during pyrolysis of different carbon content precursors.

2. Experimental part

2.1. Materials synthesis and pyrolysis

Different carbon-containing polymer precursors were used to create SiOC ceramics. The chemicals included polyhydromethylsiloxane (PHMS) that contained 20.00 wt% of carbon species in the monomer unit, polyvinylmethylsiloxane (PVMS) that contained 41.86 wt% of carbon in the monomer unit, and vinyl-terminated polymethylphenylsiloxane (PMPS) that contained 61.76 wt% of carbon in the monomer unit. These chemicals were purchased from Gelest Inc. (Morrisville, PA) and used without further purification. Commercially available polysiloxane SPR-684 Polyramic®

(PSO, Starfire Systems, Inc.) that contained 59.55 wt% carbon in the monomer unit was also used as the preceramic polymer. The molecular structures of the polymer species are given in Fig. 1. A solution of 2.1–2.4 wt% platinum–divinyltetramethyldisiloxane complex in xylene (Gelest Inc.) was further diluted in toluene and used as a catalyst at 1 wt% of polymer precursors.

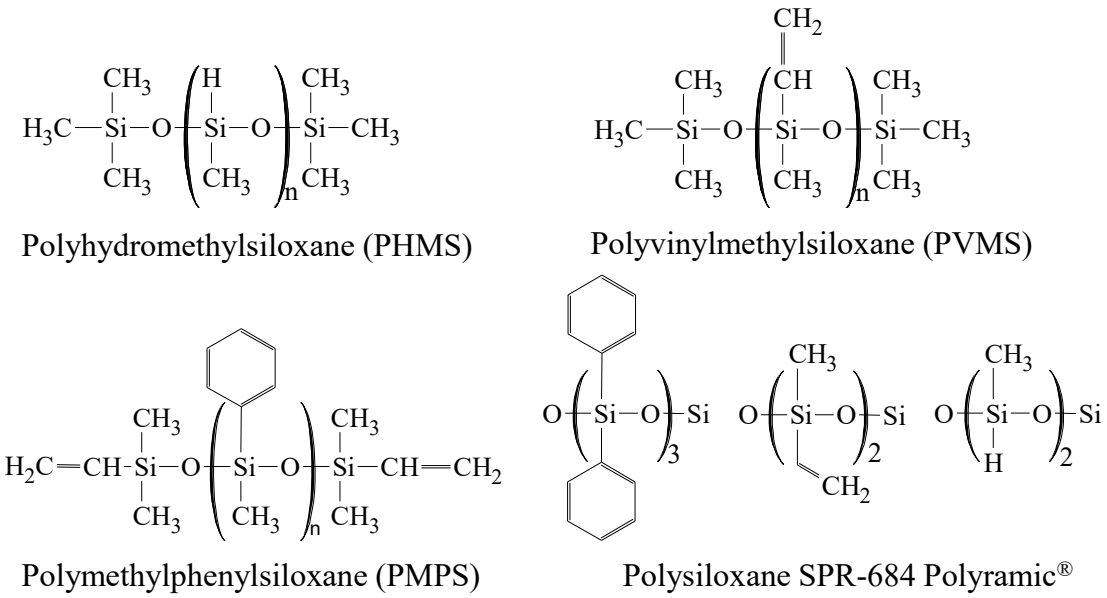

Fig. 1. Molecular structures of the polymer precursors used in this study.

85PVMS/15PHMS and 85PMPS/15PHMS samples were synthesized by the Pt-catalytic reaction between PVMS (or PMPS) and PHMS with the weight ratio of 85:15. Pure PSO was used as the single precursor. Overall, the precursor carbon content was in the order of 85PVMS/15PHMS at 38.58%, 85PMPS/15PHMS at 55.50%, and PSO at 59.55%. Specifically, for the polymer precursor crosslinking, PVMS (or PMPS) was mixed with PHMS with magnetic stirring at room temperature until a homogeneous mixture was formed. After that, a diluted (2.5 ppm) Pt catalyst solution was slowly added in the mixed solution (1 wt% relative to precursors) and magnetically stirred at 250 rpm for 2 hrs. Likewise, PSO samples were also prepared by magnetic stirring the PSO precursor and catalyst at 250 rpm for 3 hrs. Next, the corresponding solutions were poured

into cylindrical molds made by aluminum foil, respectively. The filled aluminum molds were vacuumed to remove any interior bubbles before crosslinking. The samples were first kept at 50°C for 12 hrs. After that, they were heated to 120°C and kept at this higher temperature for 12 hrs. The crosslinked samples were labeled as 85PVMS/15PHMS, 85PMPS/15PHMS, and PSO, respectively.

For pyrolysis, the 85PVMS/15PHMS, 85PMPS/15PHMS, and PSO samples were put in a ZrO_2 crucible covered by graphite paper. The crucible was then placed in a controlled atmosphere tube furnace (model No. 1730–12, CM Furnaces Inc.) for 2 hrs at two temperatures, 1200°C and 1500°C, respectively. The heating and cooling rates were kept the same at 2°C/min in a flowing Ar atmosphere.

2.2. Characterization

The synchrotron HE-XRD characterization was conducted at the 11-ID-B beamline at the Advanced Photon Source (APS, at the Argonne National Laboratory). A high-energy X-ray beam (~58 keV, λ = 0.2128 Å) was used in combination with a large amorphous silicon based area detector (PerkinElmer) to collect X-ray scattering data to high values of momentum transfer (Qmax ≈ 22 Å). The scattering images were reduced to one-dimensional data within FIT2D using CeO_2 as a calibration standard. The data were corrected for background scattering. The G(r) function was extracted from the background and Compton scattering corrected data, following Fourier transformation using PDFgetX2. The PDFs were subsequently modeled using PDFgui [48-50].

2.3. Simulation

There were multiple steps necessary to simulate the pyrolysis of a PDC system. Here, we use the PSO system as an example. The 85PVMS/15PHMS and 85PMPS/15PHMS systems

followed the same procedure. To start, an idealized linear version of the SPR-684 PSO system was created using Python, and then allowed to relax through simulation. The relaxation step was used to decrease the steric stress created by the idealized structure. During the simulation, the ReaxFF force field originally created by Van Duin et al. [43] was utilized in conjunction with LAMMPS [51], a massively parallel software used in molecular dynamics simulation. The particular force field used was provided from Van Duin's group [46] and optimized specifically for polymer-derived SiOC systems. An NPT system was created where the pressure was set to 1 MPa isostatic pressure while the temperature was set to 300 K. This allowed for the distributed polymer strands to condense and form a dense polymer. The system was allowed to rest for 20 ps with the timestep at 0.2 femtoseconds, making the total number of timesteps 100,000. After the initial densification, the system was further expanded by duplicating the linear polymer 7 times and distributing the extra chains in random orientations around the original. The system was allowed to consolidate to increase the density of the polymer system before the pyrolysis. Each polymer system was at roughly 12,000 atoms after these steps. The systems were then expanded in one last step to 90,000-100,000 atoms to allow for a larger sample size. A final consolidation step was run for 500,000 timesteps at 1 MPa isostatic pressure and 300 K. The timestep used was 0.2 fs. With the initial polymers ready, the polymer systems were ready for simulation of pyrolysis.

To simulate the pyrolysis, it became necessary to run LAMMPS integrated with Python to periodically identify and delete the gas species that would be formed during heating. The system was heated from 300 K to 2000 K in a NPT system where the Si-C bond was readily observed to be broken [47]. This took place over the course of 0.2 ns simulation time with a timestep of 0.2 fs. During this heating phase, molecules that were below the molecular weight threshold of 40 g/mol were deleted at 5 ps intervals. To accelerate the rate of bond breakage and allow for phase formation

to be observed in reasonable simulation time frames, the system was further heated to 2400 K at a much slower rate of 0.4 ns. The threshold for gas deletion was also increased to 80 g/mol at the end of the heating phase to include larger carbon species, and the interval of deletion was also increased to 10 ps. The system was then allowed to stay at 2400 K for a full nanosecond with the gas deletion criterion remaining the same. Throughout the heating phase and the temperature holding phase the pressure was increased to 2000 atm to prevent foaming of the system.

3. Results and Discussion

3.1. Phase evolution

The HE-XRD patterns for the pyrolyzed samples and illustration of the related crystal structures are shown in Fig. 2. The high-flux and high-energy X-rays enable detection of smaller length scale features because of their deep penetration and low absorption [52]. As shown in Fig. 2a, crystallite SiO_2 with an orthorhombic structure (JCPDF 00-043-0784, Fig. 2b) is detected in all the samples. This crystalline phase is the first new finding that has not been observed by conventional XRD [53-55], which can only detect amorphous SiO_2 that has a diffused halo peak at 22-23° [56] [22]. A major reason is that HE-XRD can identify diffraction peaks at <10° 2θ angles. Since synchrotron XRD can detect phase domains from the nanometer scale, it provides better sensitivity and resolution than conventional XRD. According to the persistent peak presence and distinct peak intensity that can be indexed to orthorhombic SiO_2, we believe that crystalline SiO_2 forms without the widely presumed SiOC phase separation through Eq. (3) that leads to amorphous SiO_2. This is a new finding and consistent with the absence of SiC peaks for the 85PVMS/15PHMS and 85PMPS/15PHMS samples after 1200°C pyrolysis even though they have sharper orthorhombic SiO_2 peaks. Such experimental results also mean that there is no SiOC phase

separation. The orthorhombic SiO_2 formation is fundamentally in agreement with the presence of expected tridymite phase that should be stable from 870-1470°C. SiO_2 (both orthorhombic and amorphous SiO_2) are possible in the polymer-derived SiOC systems. We believe that SiOC tetrahedrals (SiO_3C, SiO_2C_2, $SiOC_3$) form through free carbon diffusion into the SiO_2 atomic structure. This means that SiO_2 forms first and different types of SiOC tetrahedrals form after that. Eq. (3) does not exist because the amorphous SiO_2 halo does not increase with pyrolysis temperature increase.

$$\text{SiOC} \rightarrow \text{amorphous } SiO_2 + C + \text{beta-SiC} \quad (3)$$

For the samples pyrolyzed at 1200°C, a broad halo at 20.0-27.5° is detected. It can be further deconvoluted into two signals located at ~22.15° and 26.11°. The former has been reported from conventional XRD analysis [24, 57, 58] and is designated as amorphous SiO_2/SiOC tetrahedrals. This should result from the initial amorphous SiO_2 formation and diffusion of carbon into the SiO_2 open structure, leading to SiOC formation. The latter 26.11° peak belongs to the (002) plane of graphitic carbon with the P63/mmc space group (JCPDF card 00-034-0567). This halo peak right shifts for the PSO sample, meaning that the high carbon content precursor has induced more carbon diffusion into the open structure of SiO_2 and formation of carbon-rich SiOC tetrahedrals. The shifting center of the ~22.15° halo should originate from the transformation of SiO_2/SiOC tetrahedrals; the specific halo center position is a function of the relative dominance of SiO_4/SiO_3C/SiO_2C_2/$SiOC_3$ tetrahedrals. The right shift of the halos means the consumption of the oxygen-rich tetrahedrals, such as SiO_4/SiO_3C species, and formation of the carbon-rich tetrahedrals, such as SiO_2C_2 and $SiOC_3$. This observation is consistent with the results in Figs. 3 and 5 that show high C-C peaks from the RDF results. Simultaneously, orthorhombic SiO_2 is consumed and the corresponding XRD peak becomes weaker, the second finding in this study.

With the continuation of carbon diffusion into the more open-structured SiOC tetrahedrals, oxygen may be completely replaced and SiC_4 may form, as shown by the β-SiC peak at 1200°C, which is at a lower temperature than the generally accepted 1300°C for the PSO sample. Thus, the presumed separate processes for SiC formation during the SiOC formation process, SiOC phase separation and SiO_2 carbothermal reduction, are in fact a continuous and integrated process of SiO_2 and carbon carbothermal reduction. In our earlier work [15, 22, 30], phase separation was also assumed due to the lack of high resolution techniques such as HE-XRD.

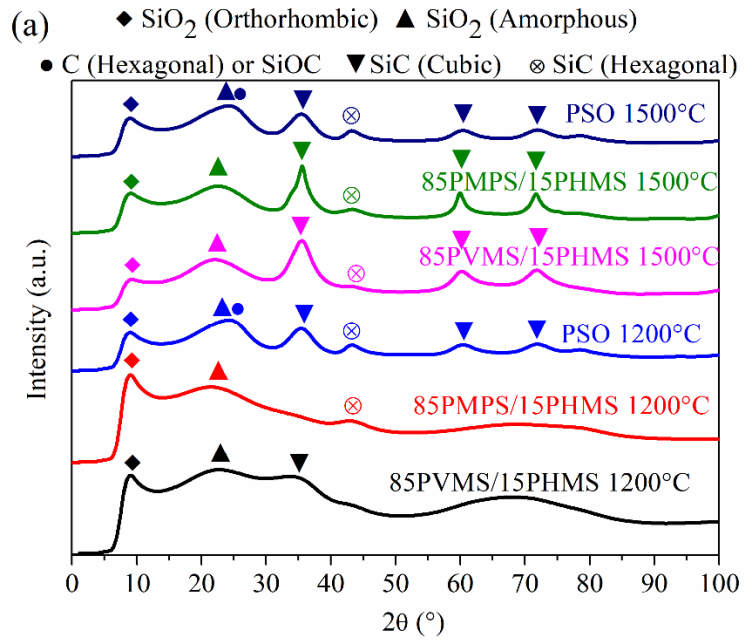

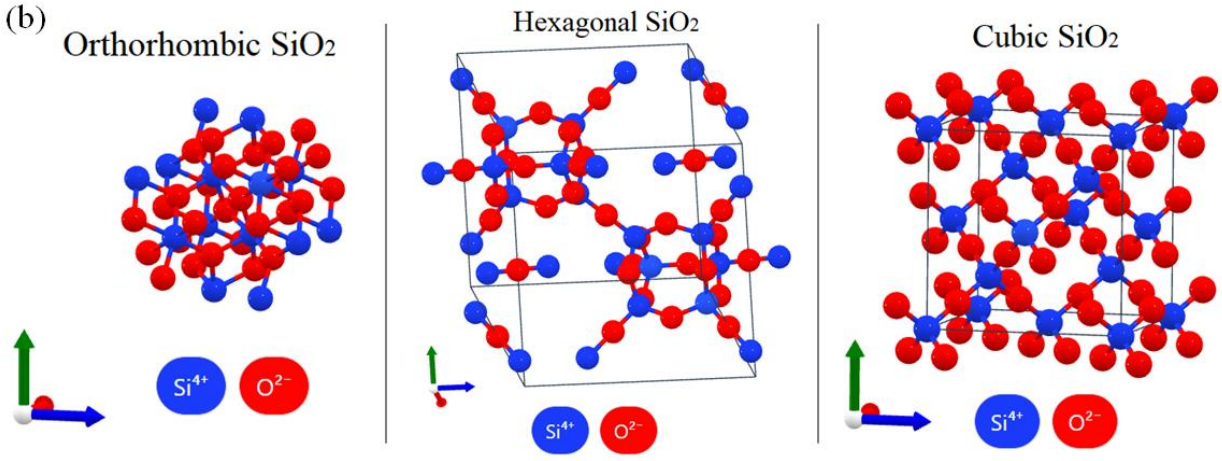

Fig. 2. a) Experimental HE-XRD data for SiOC ceramics with different carbon contents, pyrolyzed at 1200°C and 1500 °C in Ar. b) Crystal structures of different SiO_2 phases.

The third finding is that for the 1200°C pyrolyzed samples, the 85PVMS/15PHMS and 85PMPS/15PHMS samples have sharper orthorhombic SiO_2 peaks at 8.6-9.8° while the PSO sample has the most visible graphitic carbon peak. This is consistent with the carbon content difference in the precursors. For the 85PVMS/15PHMS and 85PMPS/15PHMS samples, the carbon content is lower. Thus, the orthorhombic SiO_2 peak is sharper due to the relatively higher silicon content in the precursors. For the PSO sample, the carbon content is the highest. As a result, the graphitic carbon peak is most visible. Again, such observations are consistent with the results in Figs. 3 and 5. This last observation also holds true for the 1500°C pyrolyzed samples. In addition, the samples pyrolyzed at 1500°C show weaker orthorhombic SiO_2 peaks compared to those pyrolyzed at 1200°C. This indicates that orthorhombic SiO_2 is consumed with the formation of cubic SiC through carbothermal reaction, as discussed below.

A general notion is that SiO_2 is resistant to crystallization and growth in SiOC systems, mostly staying at <5 nm size [17-19, 56, 59, 60]. This is likely because the SiO_2 phases (crystalline and amorphous) are prone to the inward diffusion of carbon during pyrolysis. Assuming that SiO_2 first forms as amorphous nanoclusters of <5 nm size, which is very likely considering the strong tendency of SiO_2 to stay amorphous/glassy, carbon diffusion causes its conversion to SiOC before it can grow and crystallize.

For the 1200°C pyrolyzed SiOC sample from PSO, cubic SiC crystallites (Fig. 2b) are detected based on the peaks at ~35, 60, and 72° 2θ angles. This phase identification is consistent with the conventional XRD data [53-55]. The fundamental process is through the well-known

carbothermal reaction between SiO_2 and carbon (Eq. 4). The SiOCs pyrolyzed from 85PVMS/15PHMS and 85PMPS/15PHMS have no discernible peaks at these 2θ angles simply because there is not enough free carbon for the carbothermal reduction.

$$\text{Amorphous } SiO_2 + C \rightarrow \beta\text{-}SiC + CO\uparrow \quad (4)$$

The much lower pyrolysis temperature (1200°C) for the cubic SiC formation is the fourth finding. From the conventional XRD analysis, the cubic SiC phase is not detected until at least 1300°C [61-64]. In this work, SiC is present at 100°C lower temperature than that reported by previous studies. This result demonstrates more sensitive phase detection capabilities from HE-XRD. More importantly, the SiC formation shows to be easier than generally known.

The last key finding is the detection of hexagonal SiC (Fig. 2b), which has not been reported in polymer-derived SiOC systems even though it is a more stable phase at the reported pyrolysis temperatures. This is likely because the cubic β-SiC crystallite size is too small and remains stable even at low temperatures. With a high carbon content (for the 1200°C pyrolyzed PSO system) or at a high pyrolysis temperature, such as 1500°C for all the samples, the cubic β-SiC crystallite size might have the tendency to grow to a large enough size (based on the sharper peak) for its phase transformation into hexagonal SiC. However, the small SiO_2 cluster size dictates the small size of the SiC crystallites, especially considering that SiC crystallites will likely be smaller because SiO_3C, SiO_2C_2, and $SiOC_3$ have to form first. For the starting PSO precursor, which has a higher carbon content than 85PVMS/15PHPS and 85PMPS/15PHPS, the formation of SiC through carbothermal reduction is more likely. Thus, the SiOC derived from PSO has the most visible SiC peaks with two SiC phases (cubic and hexagonal, Fig. 2b). For the 85PVMS/15PHPS system, only very weak cubic SiC peak is observed. However, as the precursor changes to 85PMPS/15PHPS at 1200°C, only hexagonal SiC is observed. This indicates that

hexagonal SiC can form before cubic SiC. The phase appearance is not just a function of pyrolysis temperature but also a function of Si:C ratio.

As for the samples pyrolyzed at 1500°C, the relative intensity of the diffraction peak located at 43.40° is slightly enhanced or unchanged while the 35°C peak intensity decreases with increasing carbon content from 85PVMS/15PHMS, to 85PMPS/15PHMS, and to PSO. This means that higher pyrolysis temperature decreases cubic SiC formation. Carbon content also increases the hexagonal SiC amount and decreases the cubic SiC amount dispersed in the SiOC matrix, consistent with the general thermodynamic knowledge.

3.2. Radial distribution function analysis

RDF represents probability of atomic coordination for a chosen center atom along the radial direction. By comparing the RDFs from different samples, such as by comparing the relative intensities of the peaks at different atomic coordination locations, the fine features of the atomic-scale structure and atomic coordination/bonding can be revealed, including interatomic bonding and the presence of local atomic disorder. The bond distance and coordination number can be used to analyze the phase evolution of SiOC ceramics with respect to the carbon content at different pyrolysis temperatures. The relative intensity reveals the dominance of different interatomic bonds.

The RDF data of the samples pyrolyzed at 1200℃ and 1500℃ are shown in Fig. 4. These peak positions are consistent with those reported in other studies, such as 1.42, 1.60, and 1.87 Å for C-C, Si-O and Si-C bonds respectively [65, 66]. All the bonds confirm the phases obtained from the HE-XRD results.

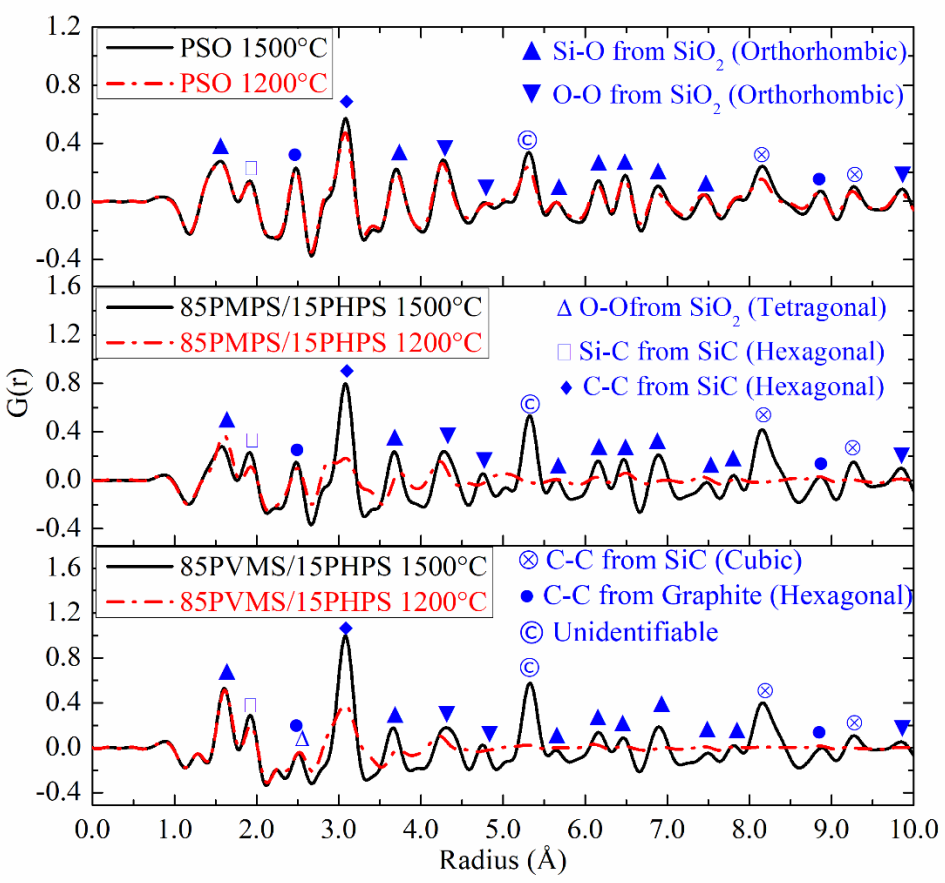

Fig. 3. RDFs of the three polymer precursors after pyrolysis at different temperatures.

At 1200°C pyrolysis temperature, Si-O bond and O-O bond from orthorhombic SiO_2, Si-C bond from hexagonal SiC, C-C bond from graphitic C, and C-C bond from hexagonal SiC are detected. For the 85PVMS/15PHMS sample after 1200°C pyrolysis, the O-O bond from tetragonal SiO_2 is observed due to its more silicon-rich nature in the precursor. Out of the three precursor systems, the PSO system has the most defined RDF peaks at 1200°C, showing the most ordered atomic coordination.

As the pyrolysis temperature is increased to 1500°C, two major changes are observed. First, more C-C bonds of hexagonal SiC form, which has not been detected for such SiOC systems in conventional studies. The same is true for the Si-O and O-O bonds of orthorhombic SiO_2. In the

g(r) curve, the C-C bond peak from hexagonal SiC is relatively higher in intensity than that of SiO_2 from orthorhombic SiO_2, suggesting more SiC ordering. The Si-O bond peaks in the medium radial distance range mean that the Si-containing tetrahedra are mostly corner-shared. The difference between Fig. 2 and Fig. 3 regarding orthorhombic SiO_2 is because Fig. 3 just shows the O-O bond intensity, not necessary the orthorhombic SiO_2 phase amount. Some O-O bonds could come from the long-range bonds in SiOC, especially considering the relatively lower intensity of the Si-O bond for the 85PVMS/15PHMS sample pyrolyzed at 1500°C. For the 85PMPS/15PHMS sample, the Si-O bond peak for the orthorhombic SiO_2 peak slightly decreases, consistent with the HE-XRD result in Fig. 2 that shows the decreasing peak intensity of the crystalline SiO_2. In addition, the graphitic C-C bond peak intensity at 2.48 Å consistently increases from 85PVMS/15PHMS to the 85PMPS/15PHMS and then to PSO, reflecting the increasing carbon-rich nature for the three systems. The intensity increases for the Si-C and C-C bonds from hexagonal SiC and the Si-O and O-O bonds from orthorhombic SiO_2 at 1500°C pyrolysis simply indicate long-range ordering and thus increased crystallinity of the systems. The PSO sample has the least bond peak changes except for slight C-C bond intensity increase for hexagonal SiC. The less long-range ordering development for PSO after 1500°C pyrolysis is due to the already developed ordering (considering the high intensity bond peaks, especially in the long range) and the carbon-rich nature of the system, which may have hindered further atomic diffusion.

It should be noted that at 1200°C pyrolysis temperature, atomic ordering has no direct correlation with the starting precursor carbon content. 85PMPS/15PHMS has similar (or slightly poorer) atomic ordering compared to 85PVMS/15PHMS even though its initial carbon content is close to that of PSO. Also, under 1200°C pyrolysis temperature, there is no medium range ordering beyond 5 Å radial distance for 85PVMS/15PHMS and 85PMPS/15PHMS, which confirms the

largely amorphous nature of these SiOC systems. For the PSO system, however, medium range ordering is observed between 5-10 Å. After 1500°C pyrolysis, the number of RDF peaks and the peak intensities are similar for all the three systems with medium range ordering. Besides, all the peak intensities increase after the pyrolysis temperature increases to 1500°C, which means improved ordering and thus higher crystallinity in the systems.

Empirically, to produce SiOC with more predictability, precursors of exact molecular structures would be desired. Commercial precursors often do not offer the exact molecular structure or composition. Pyrolysis atmosphere and duration, including specific gas partial pressure, should be quantified. The heating rate should be slow, such as 1-2°C/min, in order to provide sufficient time for complete gas release and thus composition control. The holding time at peak temperature for each pyrolysis run should also be specified.

3.3. Reactive force field modeling

The above phase evolution and RDF analyses are for SiOC systems that have undergone significant atomic structure changes. However, starting from polymer precursor decomposition, many atomic changes would have occurred. The challenge is a lack of means for understanding and quantifying the differences. ReaxFF simulation provides direct data on atomic mixing, elemental separation, and effects of precursor molecular structures and compositions, especially in the early stage of the pyrolysis. In this work, the ReaxFF simulation data can be used to reveal the atomic structure changes and new bond formation before the experimental techniques are applicable, especially in the early stage of the pyrolysis process.

Atomic structures of the ReaxFF simulated polymer systems are given in Fig. 4. Figs. 4(a-c) show that at the beginning of the pyrolysis, all the systems have a homogeneous atomic structure with no distinct features. There are small fractals of Si-O clusters throughout each system. The

amounts of the atomic species reflect the precursor compositions, with the lowest carbon content for the 85PVMS/15PHMS system and the highest amount for the PSO system (also close to that of the 85PMPS/15PHMS system). For the 85PMPS/15PHMS and PSO systems, small six-carbon rings are prevalent, reflecting their carbon-rich nature.

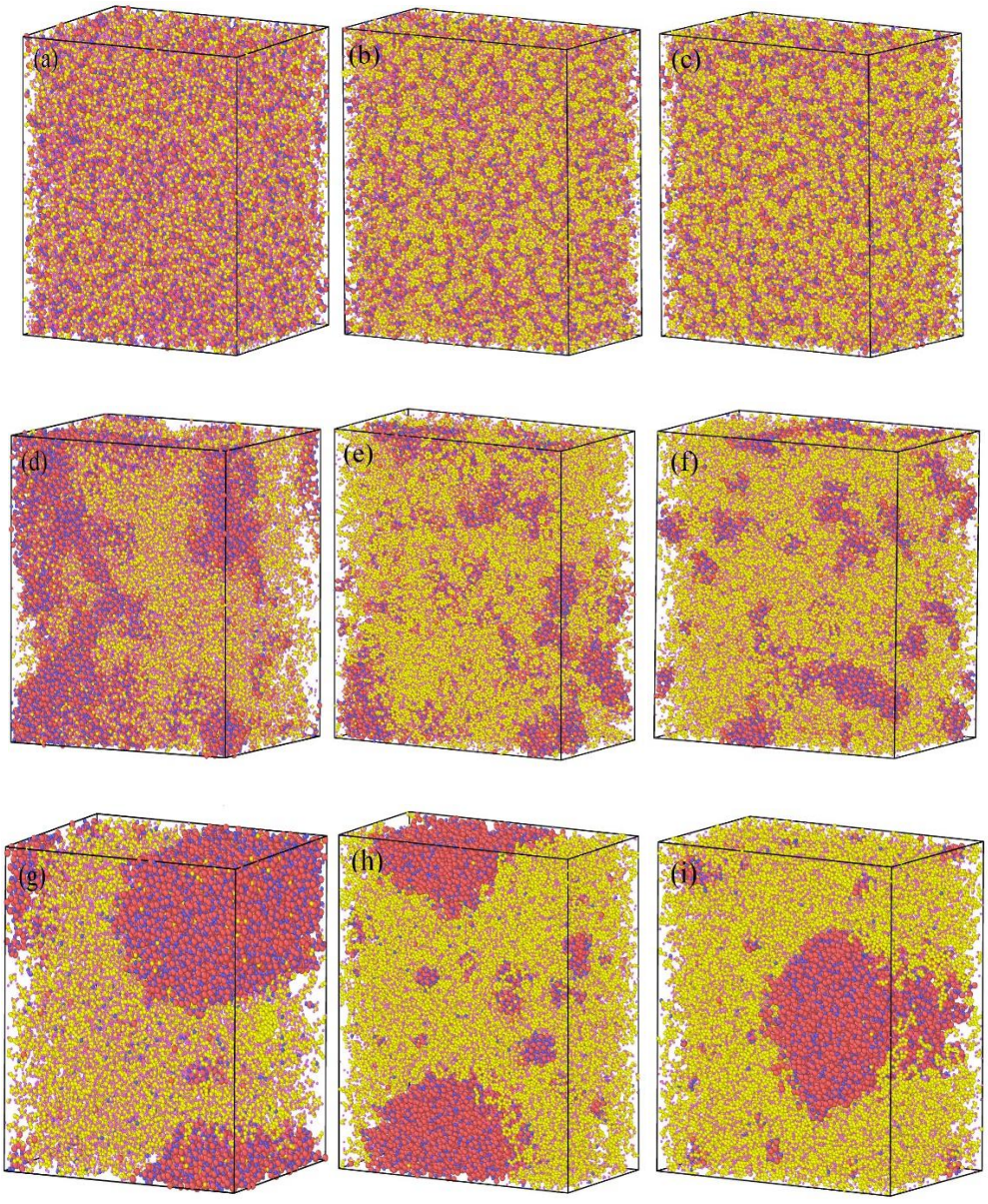

Fig. 4. Images for the 85PVMS/15PHMS, 85PMPS/15PHMS, and PSO systems at the starting state (a-c respectively), after 1800 K pyrolysis (d-f respectively), and after 2100 K pyrolysis (g-i

respectively). In all the images, the color scheme is as follows: Si-red, O-blue, C-yellow, and H-pink.

After the pyrolysis simulation at 1800 K (Figs. 4d-4f), a large amount of H is still present in all the systems, indicating that all the systems are still in the early stage of the pyrolysis process. Si-O rich and carbon-rich clusters separate. The 85PVMS/15PHMS system has less prominent carbon regions than 85PMPS/15PHMS and PSO as well as larger and less dispersed Si-O phase domains than the other two systems. In addition, the 85PVMS/15PHMS system has more carbon species still mixed in the Si-O clusters. This means that the Si-C bond in the PVMS is less likely to break. Si-O from the Si-O chains and the Si-C bond with the side group co-exist (Fig. 4d). The 85PMPS/15PHMS and PSO systems have very similar atomic structures, Si-O rich clusters are smaller in size and more dispersed. Many six-carbon rings can be observed in these two carbon-rich systems, reflecting the impact from the phenyl group in the polymer precursors. These six-carbon rings serve as the initiation units for turbostratic carbon formation. From Figs. 4d-f, it can be stated that the elemental ratios and the polymer molecular structures simultaneously influence the atomic evolution, with the elemental ratio being more significant in this study due to the large difference in Fig. 4d compared to Figs. 4e and 4f.

As the simulation temperature increases to 2100 K, there is more phase separation observed for each system (Figs. 4g-i). Compared to the 1800 K atomic structures, the simulation temperature of 2100 K results in more phase separation and larger Si-O rich clusters. The lower carbon system of 85PVMS/15PHMS has the largest carbon region and Si-O regions, with some carbon species remaining in the Si-O rich clusters. The 85PMPS/15PHMS and PSO systems have almost no carbon left in the Si-O rich regions. The Si-O rich regions continue to grow with some smaller

cluster scattered in the carbon-rich matrix. This again illustrates the effects of the precursor side groups. There is less Si-C bond breaking tendency when the side group is of small size, such as for 85PVMS/15PHPS. The phenyl group instead separates more easily and leads to more complete carbon separation from the Si-O clusters. The carbon regions in the 85PMPS/15PHMS and PSO systems have lower levels of hydrogen content. This is due to the phenyl side group in the starting precursors, which require less energy to form graphitic carbon species. Many six-carbon rings have morphed into string-like carbon units, a sign of graphene and thus turbostratic carbon formation. Again, both the precursor composition and the molecular structure affect the phase separation, with the precursor composition being more significant.

To understand the atomic bonding and coordination evolution during the early stage of pyrolysis, the RDF results for each polymer system at both 1800 K and 2100 K are given in Fig. 5. The results are extracted by examining the nature of every bond in each simulation system. This numerical bond counting is valuable in that C-H bond can be precisely counted and thus offer accurate description of the atomic coordination. The 85PVMS/15PHMS system is different from the other two higher carbon systems while the peak positions for the 85PMPS/15PHMS and PSO systems are nearly identical at both temperatures. This is likely due to the similarities in carbon contents and the presence of some similar side groups for the latter two starting precursor systems. Compared to Fig. 3, the most striking observation is that the C-H bond is present in all the polymer systems with the 85PVMS/15PHMS having the most intense peak out of the three systems. This reflects the limited time duration with molecular dynamics simulation, which makes the total deletion of hydrogen atoms prohibitive. The C-H bond peak is strongest for the 85PVMS/15PHMS system because of its low carbon content nature and less tendency of forming C-C bonds.

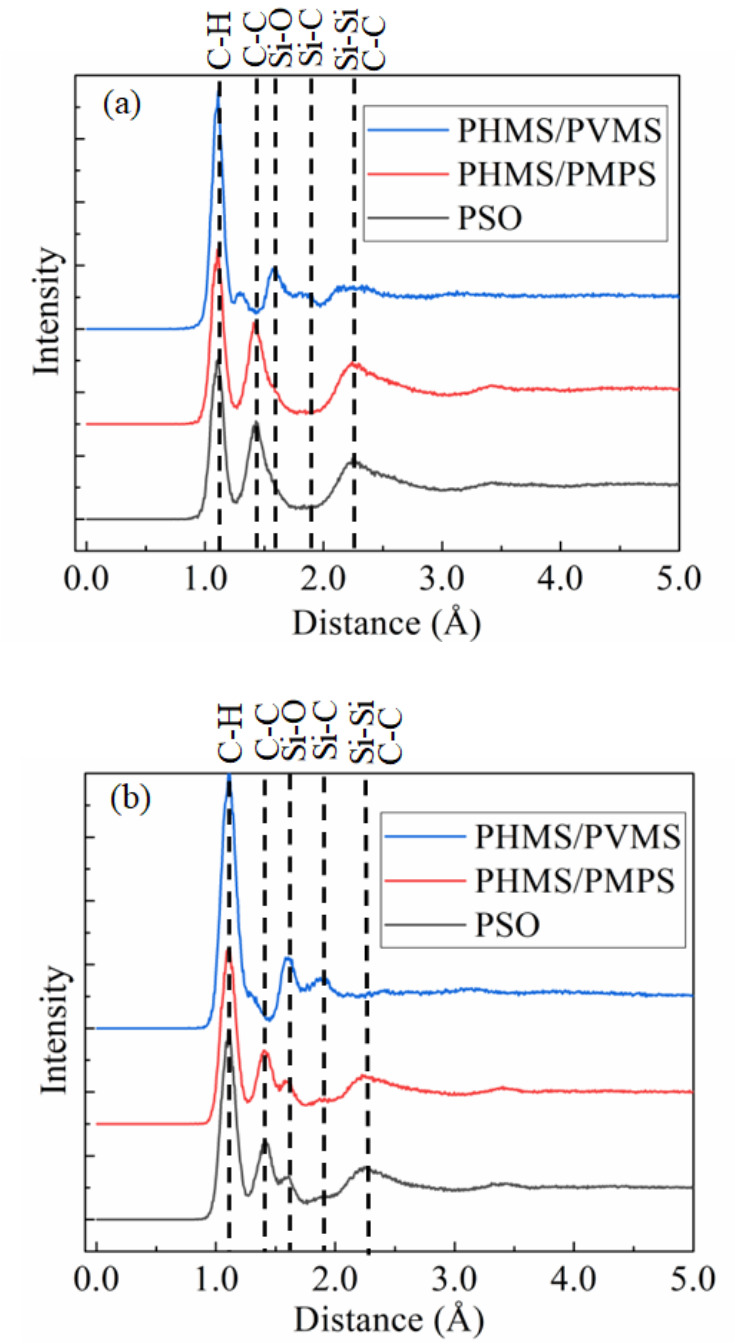

Fig. 5. RDF plots showing the 1800 K (a) and 2100 K (b) results for the three polymer systems studied.

At 1800 K, the 85PVMS/15PHMS system (Fig. 5a) has no C-C bond peaks from the inner shell at ~1.41 Å. Only a weak peak appears at the outer shell of ~2.2 Å. This is consistent with

Figs. 4d and g in that carbon co-exists with hydrogen in the carbon-rich regions. The Si-C bond is weakly present while the Si-O bond is present only for the 85PVMS/15PHMS system. The C-C bond peak from the inner shell at ~1.41 Å can be observed for the 85PMPS/15PHMS and PSO systems. This is consistent with the Si-O rich nature for the 85PVMS/15PHMS system and the carbon-rich nature for the other two systems. The ReaxFF simulation captures the atomic evolution that is not experimentally observable. The observations also support the lower tendency of Si-C bond breaking in the 85PVMS/15PHMS system due to the small size of the side groups. This means the lower tendency of the vinyl group separation from the Si-O chain. Si-C bonds are maintained at higher levels in the 85PVMS/15PHMS system.

At 2100 K (Fig. 5b), the Si-O peak appears but is still much smaller than the C-C peak for the 85PMPS/15PHMS and PSO systems. This demonstrates the continuing phase separation for all the systems. The Si-Si/C-C peak remains absent for the 85PVMS/15PHMS system and may have some slight decrease for the other two systems. This means that direct C-C bond and even Si-C bond (inner shell) are forming, indicating the early stage of atomic evolution with very limited short-range ordering. The 85PVMS/15PHMS polymer contains no cyclical carbon groups. It has significantly lower levels of C-C bond formation, suggesting that cyclical carbon groups play a large role in the creation of graphitic carbon. The similarities in atomic structure evolution for 85PMPS/15PHMS and PSO are consistent with those in the carbon content and side groups. 85PMPS/15PHMS and PSO both have significant levels of cyclical carbon side groups, which leads to more break-up of the Si-C bond in the early stage of pyrolysis.

Regarding the overlapping Si-Si and C-C bond peaks at 2.2 Å, the Si-Si bond formation is believed to be from the intermediate species of the Si-O fractals in the early stage of the pyrolysis. Since the ReaxFF simulation tracks the nature of each bond, we can compare the relative amount

of the Si-Si and C-C bonds. After 1800 K pyrolysis, both the Si-Si bond and C-C bond contents increase, with the C-C bond content taking the majority for all three precursor systems. After 2100 K pyrolysis, the C-C bond content is still predominant for the 85PMPS/15PHMS and PSO systems. However, the bond content differences become smaller. For the 85PVMS/15PHMS system, the Si-Si bond C-C bond contents are comparable, reflecting the more Si-rich nature of the polymer precursor.

4. Conclusions

SiOC has intrinsically complex microstructures that are difficult to quantify. This study focuses on the cluster evolution, phase separation, and atomic coordination through HE-XRD and RDF. We have also advanced a new ReaxFF molecular dynamics approach to understand the atomic bonding and structural evolution in the early pyrolysis process. The work for the first time shows that orthorhombic SiO_2 forms in the SiOC systems during pyrolysis and converts to amorphous SiO_2 as phase evolution continues. Cubic β-SiC also forms at lower temperatures than commonly known along with a minor amount of hexagonal SiC that has never been reported. The RDF results further support the above observations. ReaxFF simulation directly illustrates atomic mixing and separation. The simulated RDF data reveal the significant presence of C-H bonds along with Si-O and C-C bonds in the early stage of the pyrolysis.

Acknowledgments

The authors would like to acknowledge the financial support from National Science Foundation under Grant No. CBET-2024546 and Air Force Office of Scientific Research under grant number FA9550-22-1-0081. We also acknowledge the HE-XRD characterization work at the Advanced Photon Source (APS at the Argonne National Laboratory).

Data availability:

The raw data required to reproduce these findings are available to download from https://data.lib.vt.edu. The processed data required to reproduce these findings are available to download from https://data.lib.vt.edu.

References:

[1] Ahilan V, Wilhelm M, Rezwan K. Porous polymer derived ceramic (PDC)-montmorillonite-$H_3PMo_{12}O_{40}/SiO_2$ composite membranes for microbial fuel cell (MFC) application. Ceramics International. 2018;44(16):19191-9.

[2] Scheffler F, Zampieri A, Schwieger W, Zeschky J, Scheffler M, Greil P. Zeolite covered polymer derived ceramic foams: Novel hierarchical pore systems for sorption and catalysis. Advances in Applied Ceramics. 2005;104(1):43-8.

[3] Torrey JD, Bordia RK. Processing of polymer- derived ceramic composite coatings on steel. Journal of the American Ceramic Society. 2008;91(1):41-5.

[4] Nagaiah N, Kapat J, An L, Chow L. Novel polymer derived ceramic-high temperature heat flux sensor for gas turbine environment. Journal of Physics: Conference Series: IOP Publishing; 2006. p. 458.

[5] Schulz M. Polymer derived ceramics in MEMS/NEMS–A review on production processes and application. Advances in Applied Ceramics. 2009;108(8):454-60.

[6] Grossenbacher J, Gullo MR, Grandjean R, Kiefer T, Brugger J. Sub micrometer ceramic structures fabricated by molding a polymer-derived ceramic. Microelectronic Engineering. 2012;97:272-5.

[7] Francis A. Progress in polymer-derived functional silicon-based ceramic composites for biomedical and engineering applications. Materials Research Express. 2018;5(6):062003.

[8] Arango-Ospina M, Xie F, Gonzalo-Juan I, Riedel R, Ionescu E, Boccaccini AR. Silicon oxycarbide based materials for biomedical applications. Applied Materials Today. 2020;18:100482.

[9] Duan WY, Yin XW, Ye F, Li Q, Han MK, Liu XF, et al. Synthesis and EMW absorbing properties of nano SiC modified PDC-SiOC. Journal of Materials Chemistry C. 2016;4(25):5962-9.

[10] Jia YJ, Ajayi TD, Roberts MA, Chung CC, Xu CY. Ultrahigh-temperature ceramic-polymer-derived SiOC ceramic composites for high-performance electromagnetic interference shielding. ACS Applied Materials & Interfaces. 2020;12(41):46254-66.

[11] Torrey JD. Polymer derived ceramic composites as environmental barrier coatings on steel, 2006, PhD thesis.

[12] Yang N, Gao M, Li J, Lu K. Nickel- containing magnetoceramics from water vapor- assisted pyrolysis of polysiloxane and nickel 2, 4- pentanedionate. Journal of the American Ceramic Society. 2020;103(1):145-57.

[13] Yang N, Lu K. Porous and ultrahigh surface area SiOC ceramics based on perhydropolysilazane and polysiloxane. Microporous and Mesoporous Materials. 2020:110477.

[14] Lu K, Li J. Fundamental understanding of water vapor effect on SiOC evolution during pyrolysis. Journal of the European Ceramic Society. 2016;36(3):411-22.

[15] Lu K, Erb D, Bawane K, Yang N. Comparison of traditional and flash pyrolysis of different carbon content silicon oxycarbides. Journal of the European Ceramic Society. 2019;39(10):3035-41.

[16] Colombo P. Polymer derived ceramics: From nano-structure to applications: DEStech Publications, Inc; 2010.

[17] Li JK, Lu K. Highly porous SiOC bulk ceramics with water vapor assisted pyrolysis. Journaal of the American Ceramic Society. 2015;98(8):2357-65.

[18] Li JK, Lu K, Lin TS, Shen FY. Preparation of micro-/mesoporous SiOC bulk ceramics. Journal of the American Ceramic Society. 2015;98(6):1753-61.

[19] Lu K. Porous and high surface area silicon oxycarbide-based materials-A review. Materials Science and Engineering R. 2015;97:23-49.

[20] Lu K, Erb D, Liu MY. Phase transformation, oxidation stability, and electrical conductivity of TiO_2-polysiloxane derived ceramics. Journal of Materials Science. 2016;51(22):10166-77.

[21] Lu K, Li JK. Fundamental understanding of water vapor effect on SiOC evolution during pyrolysis. Journal of the European Ceramic Society. 2016;36(3):411-22.

[22] Bawane K, Erb D, Lu K. Carbon content and pyrolysis atmosphere effects on phase development in SiOC systems. Journal of the European Ceramic Society. 2019;39(9):2846-54.

[23] Zheng JQ, Lu K. Electrically conductive and thermally stable SiC-TiC containing nanocomposites via flash pyrolysis. Journal of the American Ceramic Society. 2021;104(6):2460-71.

[24] Erb D, Lu K. Additive and pyrolysis atmosphere effects on polysiloxane-derived porous SiOC ceramics. Journal of the European Ceramic Society. 2017;37(15):4547-57.

[25] Saha A, Raj R, Williamson DL. A model for the nanodomains in polymer- derived SiCO. Journal of the American Ceramic Society. 2006;89(7):2188-95.

[26] Mera G, Tamayo A, Nguyen H, Sen S, Riedel R. Nanodomain structure of carbon- rich silicon carbonitride polymer- derived ceramics. Journal of the American Ceramic Society. 2010;93(4):1169-75.

[27] Lipowitz J, Rabe JA, Frevel LK, Miller RL. Characterization of nanoporosity in polymer-derived ceramic fibres by X-ray scattering techniques. Journal of Materials Science. 1990;25(4):2118-24.

[28] Sorarù GD, Modena S, Guadagnino E, Colombo P, Egan J, Pantano C. Chemical durability of silicon oxycarbide glasses. Journal of the American Ceramic Society. 2002;85(6):1529-36.

[29] Anand R, Sahoo SP, Nayak BB, Behera SK. Phase evolution, nanostructure, and oxidation resistance of polymer derived SiTiOC ceramic hybrid. Ceramics International. 2019;45(5):6570-6.

[30] Erb D, Lu K. Synthesis of SiOC using solvent-modified polymer precursors. Materials Chemistry and Physics. 2019;237:121844.

[31] Sharma A, Hesterberg D. 9 - Synchrotron radiation-based spatial methods in environmental biogeochemistry. In: Duarte RMBO, Duarte AC, editors. Multidimensional Analytical Techniques in Environmental Research: Elsevier; 2020. p. 231-65.

[32] Liao N, Xue W, Zhang M. Effect of carbon content on structural and mechanical properties of SiCN by atomistic simulations. Journal of the European Ceramic Society. 2012;32(6):1275-81.

[33] Amkreutz M, Frauenheim T. Understanding precursor-derived amorphous Si-C-N ceramics on the atomic scale. Physical Review B. 2002;65(13):134113.

[34] Resta N, Kohler C, Trebin H-R. Molecular dynamics simulations of amorphous Si–C–N ceramics: Composition dependence of the atomic structure. Journal of the American Ceramic Society. 2003;86(8):1409-14.

[35] Tomar V, Gan M, Kim H. Atomistic analyses of the effect of temperature and morphology on mechanical strength of Si-C-N and Si-C-O nanocomposites. Journal of the European Ceramic Society. 2010;30:2223-37.

[36] Matsunaga K, Iwamoto Y, Fisher CA, Matsubara H. Molecular dynamics study of atomic structures in amorphous Si-C-N ceramics. Journal of the Ceramic Society of Japan. 1999;107(1251):1025-31.

[37] Tersoff J. Modeling solid-state chemistry: Interatomic potentials for multicomponent systems. Physical Review B. 1989;39(8):5566.

[38] Resta N, Kohler C, Trebin HR. Molecular dynamics simulations of amorphous Si–C–N ceramics: composition dependence of the atomic structure. Journal of the American Ceramic Society. 2003;86(8):1409-14.

[39] Zhang M, Liao NB, Xue W, Yang P. Large-scale molecular dynamics modeling of boron-doped amorphous SiCO ceramics. Journal of Molecular Modeling. 2017;23(6):178.

[40] Zhang M, Liao N, Xue W, Yang P. Large-scale molecular dynamics modeling of boron-doped amorphous SiCO ceramics. Journal of Molecular Modeling. 2017;23(6):178.

[41] Senftle TP, Hong S, Islam MM, Kylasa SB, Zheng Y, Shin YK, et al. The ReaxFF reactive force-field: development, applications and future directions. npj Computational Materials. 2016;2(1):15011.

[42] Newsome DA, Sengupta D, Foroutan H, Russo MF, van Duin ACT. Oxidation of silicon carbide by O_2 and H_2O: A ReaxFF reactive molecular dynamics study, Part I. The Journal of Physical Chemistry C. 2012;116(30):16111-21.

[43] van Duin ACT, Dasgupta S, Lorant F, Goddard WA. ReaxFF: A Reactive Force Field for hydrocarbons. The Journal of Physical Chemistry A. 2001;105(41):9396-409.

[44] Vashisth A, Khatri S, Hahn SH, Zhang WW, van Duin ACT, Naraghi M. Mechanical size effects of amorphous polymer-derived ceramics at the nanoscale: Experiments and ReaxFF simulations. Nanoscale. 2019;11(15):7447-56.

[45] Gao HF, Wang HJ, Zhao ZH, Niu M, Su L, Wei Y. Reactive dynamics simulation study on the pyrolysis of polymer precursors to generate amorphous silicon oxycarbide structures. Journal of Physical Chemistry C. 2018;122(10):5767-73.

[46] Ponomarev I, van Duin ACT, Kroll P. Reactive Force Field for simulations of the pyrolysis of polysiloxanes into silicon oxycarbide ceramics. Journal of Physical Chemistry C. 2019;123(27):16804-12.

[47] Chenoweth K, Cheung S, Van Duin ACT, Goddard WA, Kober EM. Simulations on the thermal decomposition of a poly(dimethylsiloxane) polymer using the ReaxFF Reactive Force Field. Journal of the American Chemical Society. 2005;127(19):7192-202.

[48] Li W, Fukunishi M, Morgan BJ, Borkiewicz OJ, Chapman KW, Pralong V, et al. A reversible phase transition for sodium insertion in anatase TiO_2. Chemistry of Materials. 2017;29(4):1836-44.

[49] Jung H, Allan PK, Hu Y-Y, Borkiewicz OJ, Wang X-L, Han W-Q, et al. Elucidation of the local and long-range structural changes that occur in germanium anodes in lithium-ion batteries. Chemistry of Materials. 2015;27(3):1031-41.

[50] Koketsu T, Ma J, Morgan BJ, Body M, Legein C, Dachraoui W, et al. Reversible magnesium and aluminium ions insertion in cation-deficient anatase TiO_2. Nature Materials. 2017;16(11):1142-8.

[51] Aktulga HM, Fogarty JC, Pandit SA, Grama AY. Parallel reactive molecular dynamics: Numerical methods and algorithmic techniques. Parallel Computing. 2012;38(4-5):245-59.

[52] Ren Y. High-energy synchrotron X-ray diffraction and its application to in situ structural phase-transition studies in complex sample environments. JOM. 2012;64(1):140-9.

[53] Singh SKD, Lu K. SiOC coatings on yttria stabilized zirconia microspheres using a fluidized bed coating process. Powder Technology. 2022;396:158-66.

[54] Rau AV, Knott K, Lu K. Porous SiOC/SiC ceramics via an active-filler-catalyzed polymer-derived method. Materials Chemistry Frontiers. 2021;5(17):6530-45.

[55] Yang N, Lu K. Effects of transition metals on the evolution of polymer-derived SiOC ceramics. Carbon. 2021;171:88-95.

[56] Erb D, Lu K. Effects of SiO_2-forming additive on polysiloxane derived SiOC ceramics. Microporous and Mesoporous Materials. 2018;266:75-82.

[57] Ma R, Lu K, Erb D. Effect of solvent in preparation of SiOC bulk ceramics. Materials Chemistry and Physics. 2018;218:140-6.

[58] Yang N, Lu K. Porous and ultrahigh surface area SiOC ceramics based on perhydropolysilazane and polysiloxane. Microporous and Mesoporous Materials. 2020;306:110477.

[59] Erb D, Lu K. Effect of additive structure and size on SiO_2 formation in polymer-derived SiOC ceramics. Journal of the American Ceramic Society. 2018;101(12):5378-88.

[60] Wen Q, Yu Z, Riedel R. The fate and role of in situ formed carbon in polymer-derived ceramics. Progress in Materials Science. 2020;109:100623.

[61] Wang LX, Lu K, Ma RX. Effects of different polymer precursors on the characteristics of SiOC bulk ceramics. Appl Phys A-Materials. 2019;125(6).

[62] Ma RX, Lu K, Erb D. Effect of solvent in preparation of SiOC bulk ceramics. Materials Chemistry and Physics. 2018;218:140-6.

[63] Liu XL, Xue JM, Ren FY, Ye F, Fan XM, Liu YS, et al. Enhanced microwave-absorption properties of polymer-derived SiC/SiOC composite ceramics modified by carbon nanowires. Ceramics International. 2020;46(13):20742-50.

[64] Mera G, Navrotsky A, Sen S, Kleebe HJ, Riedel R. Polymer-derived SiCN and SiOC ceramics - structure and energetics at the nanoscale. Journal of Materials Chemistry A. 2013;1(12):3826-36.

[65] Su Q, Inoue S, Ishimaru M, Gigax J, Wang T, Ding H, et al. Helium irradiation and implantation effects on the structure of amorphous silicon oxycarbide. Scientific Reports. 2017;7(1):3900.

[66] Ishimaru M, Bae I-T, Hirotsu Y, Matsumura S, Sickafus KE. Structural relaxation of amorphous silicon carbide. Physical Review Letters. 2002;89(5):055502.

Declaration of interests

☒ The authors declare that they have no known competing financial interests or personal relationships that could have appeared to influence the work reported in this paper.

☐The authors declare the following financial interests/personal relationships which may be considered as potential competing interests:

CRediT author statement

Harrison Chaney: Methodology, Software, Validation, Investigation, Data Curation, Writing - Original Draft, Writing - Review & Editing, Visualization

Yue Zhou: Investigation, Data Curation

Kathy Lu: Conceptualization, Methodology, Software, Validation, Formal analysis, Investigation, Resources, Writing - Original Draft, Writing - Review & Editing, Visualization, Supervision, Project administration, Funding acquisition

Understanding SiOC Atomic Structures via Synchrotron X-ray and Reactive Force Field Potential Studies

Harrison Chaney, Yue Zhou, Kathy Lu*

Department of Materials Science and Engineering, Virginia Polytechnic Institute and State University, Blacksburg, Virginia, 24061, USA

*Corresponding author: Email: klu@vt.edu

Declarations of interest: none

Abstract

Silicon oxycarbide (SiOC) is a unique system that can generate various compositions and microstructures via different polymeric precursors and pyrolysis conditions. However, understanding of the atomic structure evolution, such as cluster formation, phase evolution, and atomic coordination, is lacking. In this study, cluster evolution and atomic coordination for different SiOC ceramics pyrolyzed at 1200°C and 1500°C were investigated by high energy X-ray diffraction (HE-XRD) and radial distribution function (RDF) analysis. A new Reactive Force Field (ReaxFF) molecular dynamics modeling approach was developed to understand nanocluster separation and early-stage atomic radial coordination. For the first time, we demonstrate that orthorhombic SiO_2 forms and converts to growth resistant amorphous SiO_2. Cubic β-SiC also forms at lower temperatures than reported, along with a minor amount of hexagonal SiC that has never been reported. The RDF data support such phase evolution understanding. ReaxFF simulation provides direct data on atomic mixing, elemental separation, and effects of precursor molecular structures and compositions, especially in the early stage of the pyrolysis. The simulated RDF data complement the experimental data, revealing the significant presence of C-H bonds along with Si-O and C-C bonds.

Keywords: Silicon oxycarbide; High-energy X-ray diffraction; Radial distribution function; ReaxFF; Atomic structure

1. Introduction

In recent years, polymer-derived ceramics (PDCs) have attracted much attention due to their wide application potentials in energy [1, 2], environmental barrier coatings [3, 4], MEMS/NEMS devices [5, 6], biomedical engineering [7, 8], and electromagnetic interference shielding [9, 10]. Compared to conventional ceramics made by powder sintering, PDCs synthesized from polymeric precursors permit lower processing temperatures and offer great flexibility in controlling component sizes, shapes, and compositions [11, 12]. One outstanding class of PDCs is silicon oxycarbide (SiOC), an intriguing system with a three-dimensional covalently bonded structure consisting of silicon, oxygen, and carbon [13-15].

The ceramization of the most common precursor, polysiloxane, in a non-oxidizing atmosphere results in the formation of SiOC ceramics, and their compositions are determined by the pyrolysis temperature [16], atmosphere [17-21], and heating method [15, 22, 23]. Broadly speaking, a variety of C-H, Si-C, and Si-O bonds cleave at less than 1000°C and lead to the formation of free carbon dispersed in an amorphous SiOC matrix. When the temperature increases to 1100°C, the system is composed of amorphous SiOC clusters, free carbon, and amorphous SiO_2, which experience further microstructural evolution at higher pyrolysis temperatures and lead to the formation of nanocrystalline SiC, presumably at ≥1300°C [24]. Extensive work has been carried out to study the atomic structures of SiOC, such as by X-ray scattering and nuclear magnetic resonance (NMR) [25-27]. All the studies agree that SiOC materials contain SiC_xO_{4-x}

tetrahedra along with carbon domains, further supported by ^{13}C and ^{29}Si NMR measurements [28]. However, many studies also claim SiOC phase separation [15, 22, 29, 30] even though detailed atomic structure and phase evolution of SiOC materials remain evasive. Conventional structural characterization techniques cannot distinguish nanosized phases, atomic level clustering, and atomic coordination. Excitingly, HE-XRD experiments using a synchrotron light source offer improved sensitivity and resolution of diffraction peaks because of the high flux, tunable, and well-defined wavelength, as well as better collimation of synchrotron radiation [31]. This approach has great potential in clarifying the structural evolution of SiOC materials and obtaining new insights into the phase evolution of different nanoclusters within these materials. It can also offer atomic level radial distribution insight.

From modeling point of view, density functional theory and molecular dynamics approaches [32-35] have been used to provide the atomic structure of a precursor-derived amorphous ceramic. However, the simulated system sizes were inconsistent with the actual sizes of the phases, and the effects of chemical compositions on the evolution of these nano-sized structures need to be understood. Among several empirical potentials available for molecular dynamics (MD) simulations of covalent materials, the Tersoff potential provides a description of the crystalline and amorphous phases [36-39]. The total energy E of a system is expressed in terms of summation of atomic pair interactions V_{ij} between atoms i and j

$$E = \frac{1}{2}\sum_{i \neq j} V_{ij} \text{ where } V_{ij} = f_C(r_{ij})[f_R(r_{ij}) + b_{ij} f_A(r_{ij})] \quad (1)$$

r_{ij} is the distance from atom i to atom j. V_{ij} is composed of a repulsive part f_R and an attractive part f_A, and f_c is a smooth cutoff function to limit the range of the potential. However, for the polymer-derived pyrolysis process, such an interatomic potential is too simplistic [36-39]. There are several interatomic forces that have not been considered. For example, Zhang et al. [40] investigated the

structural features of an amorphous SiBOC ceramic by large-scale molecular dynamics (MD) calculations using the Tersoff potential, which uses a short-range pair potential to represent covalent bonding. Compared to the Tersoff potential which only considers the angular location of neighbor atoms relative to the bond axis, the ReaxFF potential [41] is more suitable for the simulation of PDCs, thanks to the consideration of a range of additional chemical bonding features, such as hydrogen bonding and bond conjugation. It is an empirical force field that allows for fully reactive atomistic scale molecular dynamics simulations of chemical reactions [42, 43]:

$$E_{\text{system}} = E_{\text{bond}} + E_{\text{over-coordination}} + E_{\text{under coordination}} + E_{\text{valence angle}} + E_{\text{penalty}} + E_{\text{torsion}} + E_{\text{conjugated energy}} + E_{\text{vdWaals}} + E_{\text{Coulomb}} \quad (2)$$

The energy potential functions associated with each of these partial energy contributions are developed by fitting against a training set comprised of both quantum mechanics (QM) and experimental data. This force field can simulate Si–C–O and Si–O–H bond interactions [44] and consider both reaction energies and reaction barriers. It allows evaluation of precursor effects on the elemental compositions, and more importantly, the phase distributions of the resulting SiOC systems. Furthermore, the ReaxFF method is several orders of magnitude faster than QM-based simulations, which enables larger-scale ($\gg$1000 atoms), fully dynamic simulations of chemical reactions [42, 43]. Thus, the ReaxFF potential approach is perceived to be more suitable for describing the tetrahedral structure of SiOC systems.

From simulation technique point of view, there has been simulation of PDCs from a bottom-up approach [45, 46], which involves the creation of the starting polymer structures. Afterwards, the system is heated and allowed to stay at highly elevated temperatures between 1800 and 2500 K where Si-C bond breakage is readily observable [47]. The pressures in the systems are kept high or the volumes are constrained to prevent the system from expanding continuously.

While the simulation is running, scripts are run periodically to selectively delete atoms belonging to smaller molecules such as methane and ethene groups (evaporative gases). However, such simulations have been carried out with relatively small systems of less than 80,000 starting atoms [40]. A more recent study with the ReaxFF approach reported amorphous end structures with comparable compositions to experiments. There was distinct phase separation between the carbon and SiOC phases [46]. Regardless, more systematic simulation work is needed in order to understand atomic structural unit evolution, radial distribution function, and bonding of different structural units.

In this study, synchrotron HE-XRD was used to explore the atomic structures and phase evolution of SiOC ceramics as a function of carbon content and pyrolysis temperature. Large-scale ReaxFF simulations were conducted to investigate the amorphous plus nanocluster structures of SiOC with different carbon content. The results from the experiments and the simulations were compared to understand the fundamental processes of the phase evolution and atomic bonding differences during pyrolysis of different carbon content precursors.

2. Experimental part

2.1. Materials synthesis and pyrolysis

Different carbon-containing polymer precursors were used to create SiOC ceramics. The chemicals included polyhydromethylsiloxane (PHMS) that contained 20.00 wt% of carbon species in the monomer unit, polyvinylmethylsiloxane (PVMS) that contained 41.86 wt% of carbon in the monomer unit, and vinyl-terminated polymethylphenylsiloxane (PMPS) that contained 61.76 wt% of carbon in the monomer unit. These chemicals were purchased from Gelest Inc. (Morrisville, PA) and used without further purification. Commercially available polysiloxane SPR-684 Polyramic®

(PSO, Starfire Systems, Inc.) that contained 59.55 wt% carbon in the monomer unit was also used as the preceramic polymer. The molecular structures of the polymer species are given in Fig. 1. A solution of 2.1–2.4 wt% platinum–divinyltetramethyldisiloxane complex in xylene (Gelest Inc.) was further diluted in toluene and used as a catalyst at 1 wt% of polymer precursors.

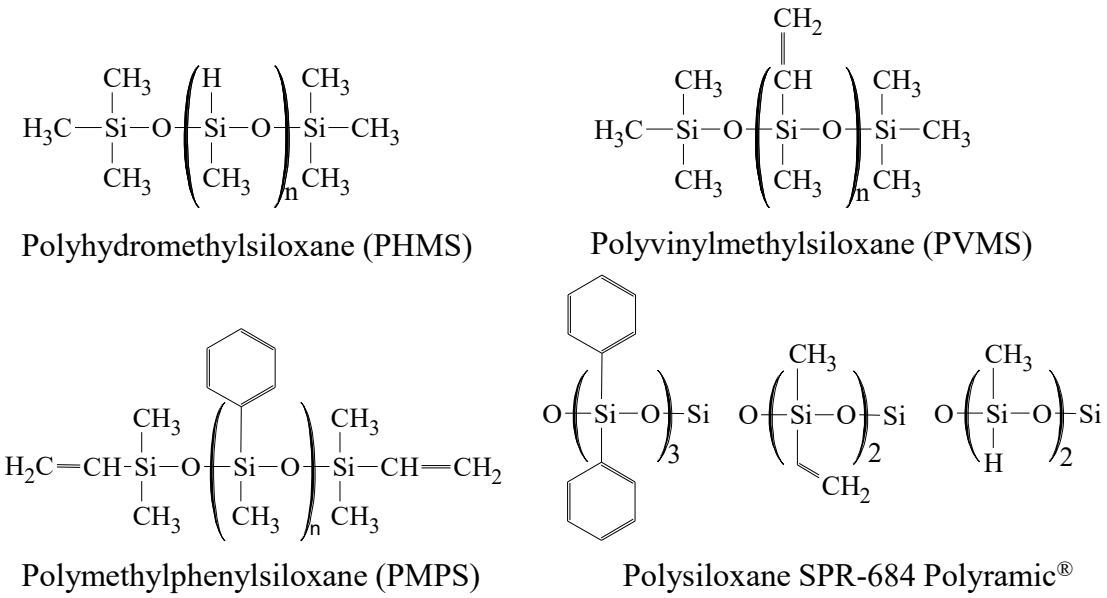

Fig. 1. Molecular structures of the polymer precursors used in this study.

85PVMS/15PHMS and 85PMPS/15PHMS samples were synthesized by the Pt-catalytic reaction between PVMS (or PMPS) and PHMS with the weight ratio of 85:15. Pure PSO was used as the single precursor. Overall, the precursor carbon content was in the order of 85PVMS/15PHMS at 38.58%, 85PMPS/15PHMS at 55.50%, and PSO at 59.55%. Specifically, for the polymer precursor crosslinking, PVMS (or PMPS) was mixed with PHMS with magnetic stirring at room temperature until a homogeneous mixture was formed. After that, a diluted (2.5 ppm) Pt catalyst solution was slowly added in the mixed solution (1 wt% relative to precursors) and magnetically stirred at 250 rpm for 2 hrs. Likewise, PSO samples were also prepared by magnetic stirring the PSO precursor and catalyst at 250 rpm for 3 hrs. Next, the corresponding solutions were poured

into cylindrical molds made by aluminum foil, respectively. The filled aluminum molds were vacuumed to remove any interior bubbles before crosslinking. The samples were first kept at 50°C for 12 hrs. After that, they were heated to 120°C and kept at this higher temperature for 12 hrs. The crosslinked samples were labeled as 85PVMS/15PHMS, 85PMPS/15PHMS, and PSO, respectively.

For pyrolysis, the 85PVMS/15PHMS, 85PMPS/15PHMS, and PSO samples were put in a ZrO_2 crucible covered by graphite paper. The crucible was then placed in a controlled atmosphere tube furnace (model No. 1730–12, CM Furnaces Inc.) for 2 hrs at two temperatures, 1200°C and 1500°C, respectively. The heating and cooling rates were kept the same at 2°C/min in a flowing Ar atmosphere.

2.2. Characterization

The synchrotron HE-XRD characterization was conducted at the 11-ID-B beamline at the Advanced Photon Source (APS, at the Argonne National Laboratory). A high-energy X-ray beam (~58 keV, λ = 0.2128 Å) was used in combination with a large amorphous silicon based area detector (PerkinElmer) to collect X-ray scattering data to high values of momentum transfer (Qmax ≈ 22 Å). The scattering images were reduced to one-dimensional data within FIT2D using CeO_2 as a calibration standard. The data were corrected for background scattering. The G(r) function was extracted from the background and Compton scattering corrected data, following Fourier transformation using PDFgetX2. The PDFs were subsequently modeled using PDFgui [48-50].

2.3. Simulation

There were multiple steps necessary to simulate the pyrolysis of a PDC system. Here, we use the PSO system as an example. The 85PVMS/15PHMS and 85PMPS/15PHMS systems

followed the same procedure. To start, an idealized linear version of the SPR-684 PSO system was created using Python, and then allowed to relax through simulation. The relaxation step was used to decrease the steric stress created by the idealized structure. During the simulation, the ReaxFF force field originally created by Van Duin et al. [43] was utilized in conjunction with LAMMPS [51], a massively parallel software used in molecular dynamics simulation. The particular force field used was provided from Van Duin's group [46] and optimized specifically for polymer-derived SiOC systems. An NPT system was created where the pressure was set to 1 MPa isostatic pressure while the temperature was set to 300 K. This allowed for the distributed polymer strands to condense and form a dense polymer. The system was allowed to rest for 20 ps with the timestep at 0.2 femtoseconds, making the total number of timesteps 100,000. After the initial densification, the system was further expanded by duplicating the linear polymer 7 times and distributing the extra chains in random orientations around the original. The system was allowed to consolidate to increase the density of the polymer system before the pyrolysis. Each polymer system was at roughly 12,000 atoms after these steps. The systems were then expanded in one last step to 90,000-100,000 atoms to allow for a larger sample size. A final consolidation step was run for 500,000 timesteps at 1 MPa isostatic pressure and 300 K. The timestep used was 0.2 fs. With the initial polymers ready, the polymer systems were ready for simulation of pyrolysis.

To simulate the pyrolysis, it became necessary to run LAMMPS integrated with Python to periodically identify and delete the gas species that would be formed during heating. The system was heated from 300 K to 2000 K in a NPT system where the Si-C bond was readily observed to be broken [47]. This took place over the course of 0.2 ns simulation time with a timestep of 0.2 fs. During this heating phase, molecules that were below the molecular weight threshold of 40 g/mol were deleted at 5 ps intervals. To accelerate the rate of bond breakage and allow for phase formation

to be observed in reasonable simulation time frames, the system was further heated to 2400 K at a much slower rate of 0.4 ns. The threshold for gas deletion was also increased to 80 g/mol at the end of the heating phase to include larger carbon species, and the interval of deletion was also increased to 10 ps. The system was then allowed to stay at 2400 K for a full nanosecond with the gas deletion criterion remaining the same. Throughout the heating phase and the temperature holding phase the pressure was increased to 2000 atm to prevent foaming of the system.

3. Results and Discussion

3.1. Phase evolution

The HE-XRD patterns for the pyrolyzed samples and illustration of the related crystal structures are shown in Fig. 2. The high-flux and high-energy X-rays enable detection of smaller length scale features because of their deep penetration and low absorption [52]. As shown in Fig. 2a, crystallite SiO_2 with an orthorhombic structure (JCPDF 00-043-0784, Fig. 2b) is detected in all the samples. This crystalline phase is the first new finding that has not been observed by conventional XRD [53-55], which can only detect amorphous SiO_2 that has a diffused halo peak at 22-23° [56] [22]. A major reason is that HE-XRD can identify diffraction peaks at <10° 2θ angles. Since synchrotron XRD can detect phase domains from the nanometer scale, it provides better sensitivity and resolution than conventional XRD. According to the persistent peak presence and distinct peak intensity that can be indexed to orthorhombic SiO_2, we believe that crystalline SiO_2 forms without the widely presumed SiOC phase separation through Eq. (3) that leads to amorphous SiO_2. This is a new finding and consistent with the absence of SiC peaks for the 85PVMS/15PHMS and 85PMPS/15PHMS samples after 1200°C pyrolysis even though they have sharper orthorhombic SiO_2 peaks. Such experimental results also mean that there is no SiOC phase

separation. The orthorhombic SiO_2 formation is fundamentally in agreement with the presence of expected tridymite phase that should be stable from 870-1470°C. SiO_2 (both orthorhombic and amorphous SiO_2) are possible in the polymer-derived SiOC systems. We believe that SiOC tetrahedrals (SiO_3C, SiO_2C_2, $SiOC_3$) form through free carbon diffusion into the SiO_2 atomic structure. This means that SiO_2 forms first and different types of SiOC tetrahedrals form after that. Eq. (3) does not exist because the amorphous SiO_2 halo does not increase with pyrolysis temperature increase.

$$\text{SiOC} \rightarrow \text{amorphous } SiO_2 + C + \text{beta-SiC} \quad (3)$$

For the samples pyrolyzed at 1200°C, a broad halo at 20.0-27.5° is detected. It can be further deconvoluted into two signals located at ~22.15° and 26.11°. The former has been reported from conventional XRD analysis [24, 57, 58] and is designated as amorphous SiO_2/SiOC tetrahedrals. This should result from the initial amorphous SiO_2 formation and diffusion of carbon into the SiO_2 open structure, leading to SiOC formation. The latter 26.11° peak belongs to the (002) plane of graphitic carbon with the P63/mmc space group (JCPDF card 00-034-0567). This halo peak right shifts for the PSO sample, meaning that the high carbon content precursor has induced more carbon diffusion into the open structure of SiO_2 and formation of carbon-rich SiOC tetrahedrals. The shifting center of the ~22.15° halo should originate from the transformation of SiO_2/SiOC tetrahedrals; the specific halo center position is a function of the relative dominance of SiO_4/SiO_3C/SiO_2C_2/$SiOC_3$ tetrahedrals. The right shift of the halos means the consumption of the oxygen-rich tetrahedrals, such as SiO_4/SiO_3C species, and formation of the carbon-rich tetrahedrals, such as SiO_2C_2 and $SiOC_3$. This observation is consistent with the results in Figs. 3 and 5 that show high C-C peaks from the RDF results. Simultaneously, orthorhombic SiO_2 is consumed and the corresponding XRD peak becomes weaker, the second finding in this study.

With the continuation of carbon diffusion into the more open-structured SiOC tetrahedrals, oxygen may be completely replaced and SiC_4 may form, as shown by the β-SiC peak at 1200°C, which is at a lower temperature than the generally accepted 1300°C for the PSO sample. Thus, the presumed separate processes for SiC formation during the SiOC formation process, SiOC phase separation and SiO_2 carbothermal reduction, are in fact a continuous and integrated process of SiO_2 and carbon carbothermal reduction. In our earlier work [15, 22, 30], phase separation was also assumed due to the lack of high resolution techniques such as HE-XRD.

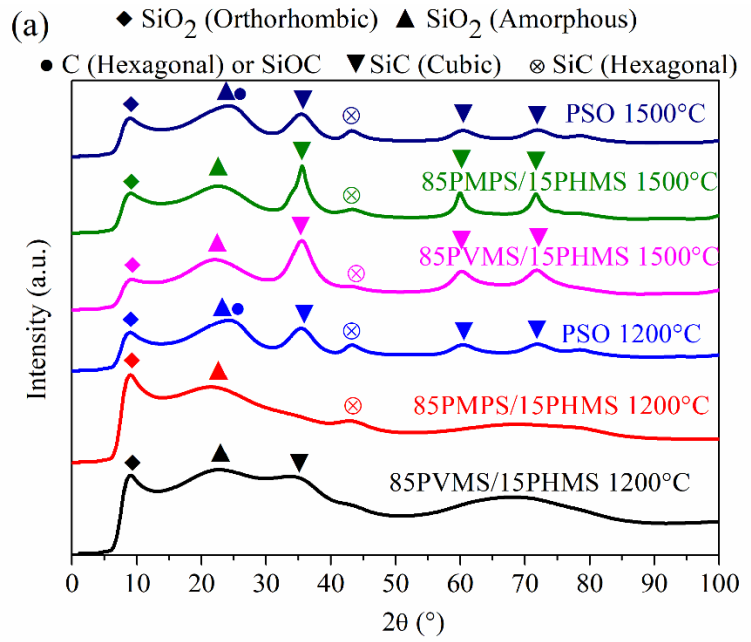

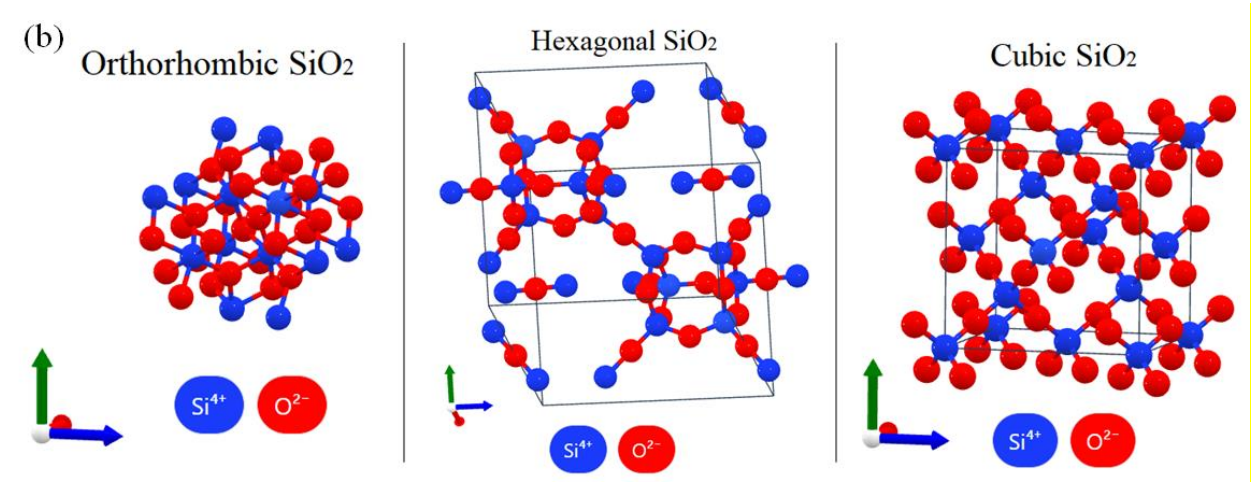

Fig. 2. a) Experimental HE-XRD data for SiOC ceramics with different carbon contents, pyrolyzed at 1200°C and 1500 °C in Ar. b) Crystal structures of different SiO_2 phases.

The third finding is that for the 1200°C pyrolyzed samples, the 85PVMS/15PHMS and 85PMPS/15PHMS samples have sharper orthorhombic SiO_2 peaks at 8.6-9.8° while the PSO sample has the most visible graphitic carbon peak. This is consistent with the carbon content difference in the precursors. For the 85PVMS/15PHMS and 85PMPS/15PHMS samples, the carbon content is lower. Thus, the orthorhombic SiO_2 peak is sharper due to the relatively higher silicon content in the precursors. For the PSO sample, the carbon content is the highest. As a result, the graphitic carbon peak is most visible. Again, such observations are consistent with the results in Figs. 3 and 5. This last observation also holds true for the 1500°C pyrolyzed samples. In addition, the samples pyrolyzed at 1500°C show weaker orthorhombic SiO_2 peaks compared to those pyrolyzed at 1200°C. This indicates that orthorhombic SiO_2 is consumed with the formation of cubic SiC through carbothermal reaction, as discussed below.

A general notion is that SiO_2 is resistant to crystallization and growth in SiOC systems, mostly staying at <5 nm size [17-19, 56, 59, 60]. This is likely because the SiO_2 phases (crystalline and amorphous) are prone to the inward diffusion of carbon during pyrolysis. Assuming that SiO_2 first forms as amorphous nanoclusters of <5 nm size, which is very likely considering the strong tendency of SiO_2 to stay amorphous/glassy, carbon diffusion causes its conversion to SiOC before it can grow and crystallize.

For the 1200°C pyrolyzed SiOC sample from PSO, cubic SiC crystallites (Fig. 2b) are detected based on the peaks at ~35, 60, and 72° 2θ angles. This phase identification is consistent with the conventional XRD data [53-55]. The fundamental process is through the well-known

carbothermal reaction between SiO_2 and carbon (Eq. 4). The SiOCs pyrolyzed from 85PVMS/15PHMS and 85PMPS/15PHMS have no discernible peaks at these 2θ angles simply because there is not enough free carbon for the carbothermal reduction.

$$\text{Amorphous } SiO_2 + C \rightarrow \beta\text{-}SiC + CO\uparrow \quad (4)$$

The much lower pyrolysis temperature (1200°C) for the cubic SiC formation is the fourth finding. From the conventional XRD analysis, the cubic SiC phase is not detected until at least 1300°C [61-64]. In this work, SiC is present at 100°C lower temperature than that reported by previous studies. This result demonstrates more sensitive phase detection capabilities from HE-XRD. More importantly, the SiC formation shows to be easier than generally known.

The last key finding is the detection of hexagonal SiC (Fig. 2b), which has not been reported in polymer-derived SiOC systems even though it is a more stable phase at the reported pyrolysis temperatures. This is likely because the cubic β-SiC crystallite size is too small and remains stable even at low temperatures. With a high carbon content (for the 1200°C pyrolyzed PSO system) or at a high pyrolysis temperature, such as 1500°C for all the samples, the cubic β-SiC crystallite size might have the tendency to grow to a large enough size (based on the sharper peak) for its phase transformation into hexagonal SiC. However, the small SiO_2 cluster size dictates the small size of the SiC crystallites, especially considering that SiC crystallites will likely be smaller because SiO_3C, SiO_2C_2, and $SiOC_3$ have to form first. For the starting PSO precursor, which has a higher carbon content than 85PVMS/15PHPS and 85PMPS/15PHPS, the formation of SiC through carbothermal reduction is more likely. Thus, the SiOC derived from PSO has the most visible SiC peaks with two SiC phases (cubic and hexagonal, Fig. 2b). For the 85PVMS/15PHPS system, only very weak cubic SiC peak is observed. However, as the precursor changes to 85PMPS/15PHPS at 1200°C, only hexagonal SiC is observed. This indicates that

hexagonal SiC can form before cubic SiC. The phase appearance is not just a function of pyrolysis temperature but also a function of Si:C ratio.

As for the samples pyrolyzed at 1500°C, the relative intensity of the diffraction peak located at 43.40° is slightly enhanced or unchanged while the 35°C peak intensity decreases with increasing carbon content from 85PVMS/15PHMS, to 85PMPS/15PHMS, and to PSO. This means that higher pyrolysis temperature decreases cubic SiC formation. Carbon content also increases the hexagonal SiC amount and decreases the cubic SiC amount dispersed in the SiOC matrix, consistent with the general thermodynamic knowledge.

3.2. Radial distribution function analysis

RDF represents probability of atomic coordination for a chosen center atom along the radial direction. By comparing the RDFs from different samples, such as by comparing the relative intensities of the peaks at different atomic coordination locations, the fine features of the atomic-scale structure and atomic coordination/bonding can be revealed, including interatomic bonding and the presence of local atomic disorder. The bond distance and coordination number can be used to analyze the phase evolution of SiOC ceramics with respect to the carbon content at different pyrolysis temperatures. The relative intensity reveals the dominance of different interatomic bonds.

The RDF data of the samples pyrolyzed at 1200℃ and 1500℃ are shown in Fig. 4. These peak positions are consistent with those reported in other studies, such as 1.42, 1.60, and 1.87 Å for C-C, Si-O and Si-C bonds respectively [65, 66]. All the bonds confirm the phases obtained from the HE-XRD results.

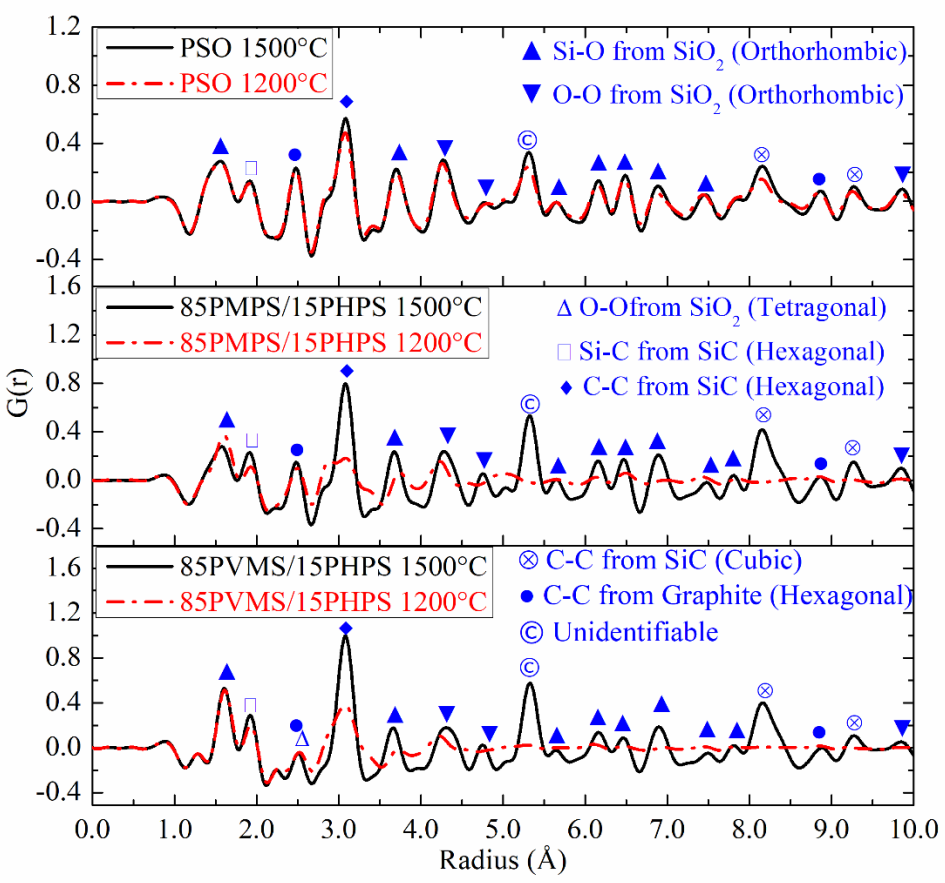

Fig. 3. RDFs of the three polymer precursors after pyrolysis at different temperatures.

At 1200°C pyrolysis temperature, Si-O bond and O-O bond from orthorhombic SiO_2, Si-C bond from hexagonal SiC, C-C bond from graphitic C, and C-C bond from hexagonal SiC are detected. For the 85PVMS/15PHMS sample after 1200°C pyrolysis, the O-O bond from tetragonal SiO_2 is observed due to its more silicon-rich nature in the precursor. Out of the three precursor systems, the PSO system has the most defined RDF peaks at 1200°C, showing the most ordered atomic coordination.

As the pyrolysis temperature is increased to 1500°C, two major changes are observed. First, more C-C bonds of hexagonal SiC form, which has not been detected for such SiOC systems in conventional studies. The same is true for the Si-O and O-O bonds of orthorhombic SiO_2. In the

g(r) curve, the C-C bond peak from hexagonal SiC is relatively higher in intensity than that of SiO_2 from orthorhombic SiO_2, suggesting more SiC ordering. The Si-O bond peaks in the medium radial distance range mean that the Si-containing tetrahedra are mostly corner-shared. The difference between Fig. 2 and Fig. 3 regarding orthorhombic SiO_2 is because Fig. 3 just shows the O-O bond intensity, not necessary the orthorhombic SiO_2 phase amount. Some O-O bonds could come from the long-range bonds in SiOC, especially considering the relatively lower intensity of the Si-O bond for the 85PVMS/15PHMS sample pyrolyzed at 1500°C. For the 85PMPS/15PHMS sample, the Si-O bond peak for the orthorhombic SiO_2 peak slightly decreases, consistent with the HE-XRD result in Fig. 2 that shows the decreasing peak intensity of the crystalline SiO_2. In addition, the graphitic C-C bond peak intensity at 2.48 Å consistently increases from 85PVMS/15PHMS to the 85PMPS/15PHMS and then to PSO, reflecting the increasing carbon-rich nature for the three systems. The intensity increases for the Si-C and C-C bonds from hexagonal SiC and the Si-O and O-O bonds from orthorhombic SiO_2 at 1500°C pyrolysis simply indicate long-range ordering and thus increased crystallinity of the systems. The PSO sample has the least bond peak changes except for slight C-C bond intensity increase for hexagonal SiC. The less long-range ordering development for PSO after 1500°C pyrolysis is due to the already developed ordering (considering the high intensity bond peaks, especially in the long range) and the carbon-rich nature of the system, which may have hindered further atomic diffusion.

It should be noted that at 1200°C pyrolysis temperature, atomic ordering has no direct correlation with the starting precursor carbon content. 85PMPS/15PHMS has similar (or slightly poorer) atomic ordering compared to 85PVMS/15PHMS even though its initial carbon content is close to that of PSO. Also, under 1200°C pyrolysis temperature, there is no medium range ordering beyond 5 Å radial distance for 85PVMS/15PHMS and 85PMPS/15PHMS, which confirms the

largely amorphous nature of these SiOC systems. For the PSO system, however, medium range ordering is observed between 5-10 Å. After 1500°C pyrolysis, the number of RDF peaks and the peak intensities are similar for all the three systems with medium range ordering. Besides, all the peak intensities increase after the pyrolysis temperature increases to 1500°C, which means improved ordering and thus higher crystallinity in the systems.

Empirically, to produce SiOC with more predictability, precursors of exact molecular structures would be desired. Commercial precursors often do not offer the exact molecular structure or composition. Pyrolysis atmosphere and duration, including specific gas partial pressure, should be quantified. The heating rate should be slow, such as 1-2°C/min, in order to provide sufficient time for complete gas release and thus composition control. The holding time at peak temperature for each pyrolysis run should also be specified.

3.3. Reactive force field modeling

The above phase evolution and RDF analyses are for SiOC systems that have undergone significant atomic structure changes. However, starting from polymer precursor decomposition, many atomic changes would have occurred. The challenge is a lack of means for understanding and quantifying the differences. ReaxFF simulation provides direct data on atomic mixing, elemental separation, and effects of precursor molecular structures and compositions, especially in the early stage of the pyrolysis. In this work, the ReaxFF simulation data can be used to reveal the atomic structure changes and new bond formation before the experimental techniques are applicable, especially in the early stage of the pyrolysis process.

Atomic structures of the ReaxFF simulated polymer systems are given in Fig. 4. Figs. 4(a-c) show that at the beginning of the pyrolysis, all the systems have a homogeneous atomic structure with no distinct features. There are small fractals of Si-O clusters throughout each system. The

amounts of the atomic species reflect the precursor compositions, with the lowest carbon content for the 85PVMS/15PHMS system and the highest amount for the PSO system (also close to that of the 85PMPS/15PHMS system). For the 85PMPS/15PHMS and PSO systems, small six-carbon rings are prevalent, reflecting their carbon-rich nature.

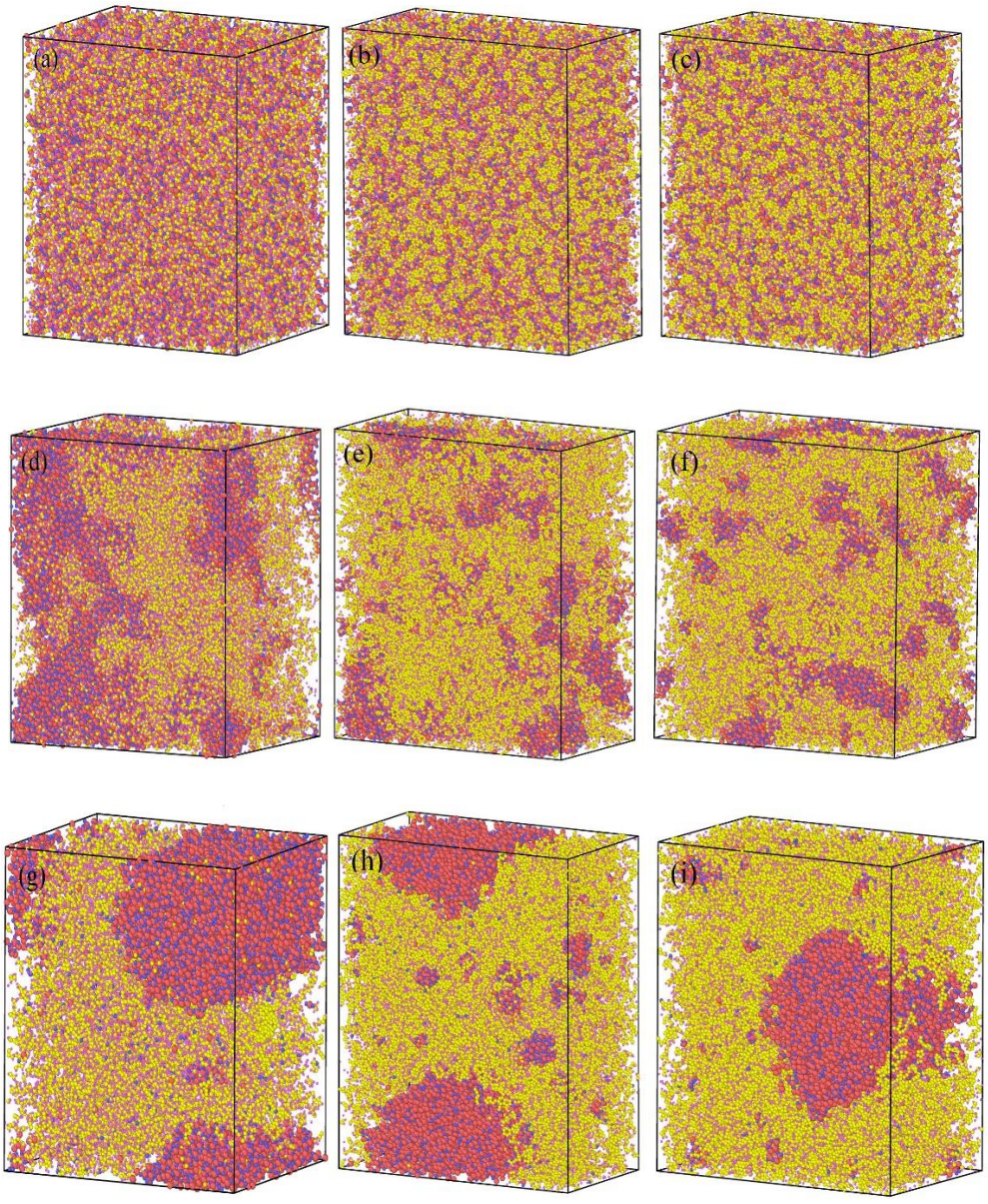

Fig. 4. Images for the 85PVMS/15PHMS, 85PMPS/15PHMS, and PSO systems at the starting state (a-c respectively), after 1800 K pyrolysis (d-f respectively), and after 2100 K pyrolysis (g-i

respectively). In all the images, the color scheme is as follows: Si-red, O-blue, C-yellow, and H-pink.

After the pyrolysis simulation at 1800 K (Figs. 4d-4f), a large amount of H is still present in all the systems, indicating that all the systems are still in the early stage of the pyrolysis process. Si-O rich and carbon-rich clusters separate. The 85PVMS/15PHMS system has less prominent carbon regions than 85PMPS/15PHMS and PSO as well as larger and less dispersed Si-O phase domains than the other two systems. In addition, the 85PVMS/15PHMS system has more carbon species still mixed in the Si-O clusters. This means that the Si-C bond in the PVMS is less likely to break. Si-O from the Si-O chains and the Si-C bond with the side group co-exist (Fig. 4d). The 85PMPS/15PHMS and PSO systems have very similar atomic structures, Si-O rich clusters are smaller in size and more dispersed. Many six-carbon rings can be observed in these two carbon-rich systems, reflecting the impact from the phenyl group in the polymer precursors. These six-carbon rings serve as the initiation units for turbostratic carbon formation. From Figs. 4d-f, it can be stated that the elemental ratios and the polymer molecular structures simultaneously influence the atomic evolution, with the elemental ratio being more significant in this study due to the large difference in Fig. 4d compared to Figs. 4e and 4f.

As the simulation temperature increases to 2100 K, there is more phase separation observed for each system (Figs. 4g-i). Compared to the 1800 K atomic structures, the simulation temperature of 2100 K results in more phase separation and larger Si-O rich clusters. The lower carbon system of 85PVMS/15PHMS has the largest carbon region and Si-O regions, with some carbon species remaining in the Si-O rich clusters. The 85PMPS/15PHMS and PSO systems have almost no carbon left in the Si-O rich regions. The Si-O rich regions continue to grow with some smaller

cluster scattered in the carbon-rich matrix. This again illustrates the effects of the precursor side groups. There is less Si-C bond breaking tendency when the side group is of small size, such as for 85PVMS/15PHPS. The phenyl group instead separates more easily and leads to more complete carbon separation from the Si-O clusters. The carbon regions in the 85PMPS/15PHMS and PSO systems have lower levels of hydrogen content. This is due to the phenyl side group in the starting precursors, which require less energy to form graphitic carbon species. Many six-carbon rings have morphed into string-like carbon units, a sign of graphene and thus turbostratic carbon formation. Again, both the precursor composition and the molecular structure affect the phase separation, with the precursor composition being more significant.

To understand the atomic bonding and coordination evolution during the early stage of pyrolysis, the RDF results for each polymer system at both 1800 K and 2100 K are given in Fig. 5. The results are extracted by examining the nature of every bond in each simulation system. This numerical bond counting is valuable in that C-H bond can be precisely counted and thus offer accurate description of the atomic coordination. The 85PVMS/15PHMS system is different from the other two higher carbon systems while the peak positions for the 85PMPS/15PHMS and PSO systems are nearly identical at both temperatures. This is likely due to the similarities in carbon contents and the presence of some similar side groups for the latter two starting precursor systems. Compared to Fig. 3, the most striking observation is that the C-H bond is present in all the polymer systems with the 85PVMS/15PHMS having the most intense peak out of the three systems. This reflects the limited time duration with molecular dynamics simulation, which makes the total deletion of hydrogen atoms prohibitive. The C-H bond peak is strongest for the 85PVMS/15PHMS system because of its low carbon content nature and less tendency of forming C-C bonds.

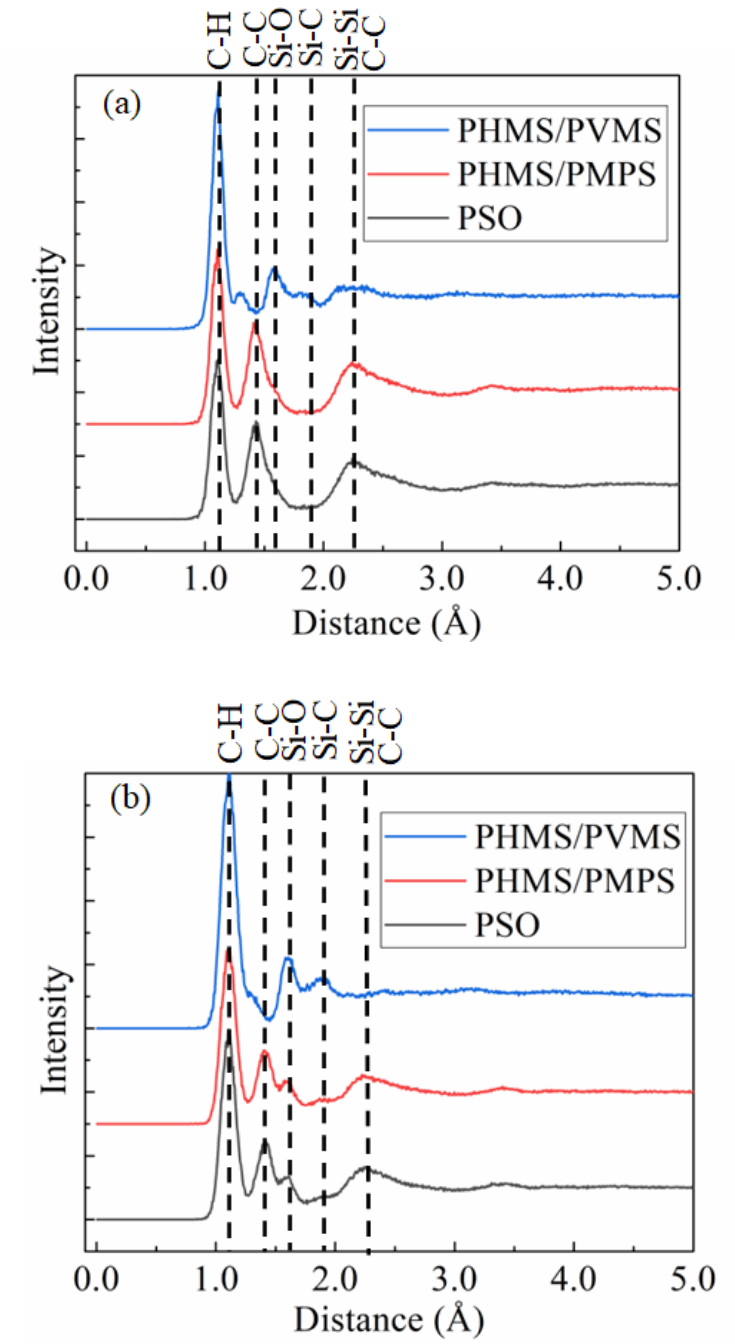

Fig. 5. RDF plots showing the 1800 K (a) and 2100 K (b) results for the three polymer systems studied.

At 1800 K, the 85PVMS/15PHMS system (Fig. 5a) has no C-C bond peaks from the inner shell at ~1.41 Å. Only a weak peak appears at the outer shell of ~2.2 Å. This is consistent with

Figs. 4d and g in that carbon co-exists with hydrogen in the carbon-rich regions. The Si-C bond is weakly present while the Si-O bond is present only for the 85PVMS/15PHMS system. The C-C bond peak from the inner shell at ~1.41 Å can be observed for the 85PMPS/15PHMS and PSO systems. This is consistent with the Si-O rich nature for the 85PVMS/15PHMS system and the carbon-rich nature for the other two systems. The ReaxFF simulation captures the atomic evolution that is not experimentally observable. The observations also support the lower tendency of Si-C bond breaking in the 85PVMS/15PHMS system due to the small size of the side groups. This means the lower tendency of the vinyl group separation from the Si-O chain. Si-C bonds are maintained at higher levels in the 85PVMS/15PHMS system.

At 2100 K (Fig. 5b), the Si-O peak appears but is still much smaller than the C-C peak for the 85PMPS/15PHMS and PSO systems. This demonstrates the continuing phase separation for all the systems. The Si-Si/C-C peak remains absent for the 85PVMS/15PHMS system and may have some slight decrease for the other two systems. This means that direct C-C bond and even Si-C bond (inner shell) are forming, indicating the early stage of atomic evolution with very limited short-range ordering. The 85PVMS/15PHMS polymer contains no cyclical carbon groups. It has significantly lower levels of C-C bond formation, suggesting that cyclical carbon groups play a large role in the creation of graphitic carbon. The similarities in atomic structure evolution for 85PMPS/15PHMS and PSO are consistent with those in the carbon content and side groups. 85PMPS/15PHMS and PSO both have significant levels of cyclical carbon side groups, which leads to more break-up of the Si-C bond in the early stage of pyrolysis.

Regarding the overlapping Si-Si and C-C bond peaks at 2.2 Å, the Si-Si bond formation is believed to be from the intermediate species of the Si-O fractals in the early stage of the pyrolysis. Since the ReaxFF simulation tracks the nature of each bond, we can compare the relative amount

of the Si-Si and C-C bonds. After 1800 K pyrolysis, both the Si-Si bond and C-C bond contents increase, with the C-C bond content taking the majority for all three precursor systems. After 2100 K pyrolysis, the C-C bond content is still predominant for the 85PMPS/15PHMS and PSO systems. However, the bond content differences become smaller. For the 85PVMS/15PHMS system, the Si-Si bond C-C bond contents are comparable, reflecting the more Si-rich nature of the polymer precursor.

4. Conclusions

SiOC has intrinsically complex microstructures that are difficult to quantify. This study focuses on the cluster evolution, phase separation, and atomic coordination through HE-XRD and RDF. We have also advanced a new ReaxFF molecular dynamics approach to understand the atomic bonding and structural evolution in the early pyrolysis process. The work for the first time shows that orthorhombic SiO_2 forms in the SiOC systems during pyrolysis and converts to amorphous SiO_2 as phase evolution continues. Cubic β-SiC also forms at lower temperatures than commonly known along with a minor amount of hexagonal SiC that has never been reported. The RDF results further support the above observations. ReaxFF simulation directly illustrates atomic mixing and separation. The simulated RDF data reveal the significant presence of C-H bonds along with Si-O and C-C bonds in the early stage of the pyrolysis.

Acknowledgments

The authors would like to acknowledge the financial support from National Science Foundation under Grant No. CBET-2024546 and Air Force Office of Scientific Research under grant number FA9550-22-1-0081. We also acknowledge the HE-XRD characterization work at the Advanced Photon Source (APS at the Argonne National Laboratory).

Data availability:

The raw data required to reproduce these findings are available to download from https://data.lib.vt.edu. The processed data required to reproduce these findings are available to download from https://data.lib.vt.edu.

References:

[1] Ahilan V, Wilhelm M, Rezwan K. Porous polymer derived ceramic (PDC)-montmorillonite-$H_3PMo_{12}O_{40}/SiO_2$ composite membranes for microbial fuel cell (MFC) application. Ceramics International. 2018;44(16):19191-9.

[2] Scheffler F, Zampieri A, Schwieger W, Zeschky J, Scheffler M, Greil P. Zeolite covered polymer derived ceramic foams: Novel hierarchical pore systems for sorption and catalysis. Advances in Applied Ceramics. 2005;104(1):43-8.

[3] Torrey JD, Bordia RK. Processing of polymer- derived ceramic composite coatings on steel. Journal of the American Ceramic Society. 2008;91(1):41-5.

[4] Nagaiah N, Kapat J, An L, Chow L. Novel polymer derived ceramic-high temperature heat flux sensor for gas turbine environment. Journal of Physics: Conference Series: IOP Publishing; 2006. p. 458.

[5] Schulz M. Polymer derived ceramics in MEMS/NEMS–A review on production processes and application. Advances in Applied Ceramics. 2009;108(8):454-60.

[6] Grossenbacher J, Gullo MR, Grandjean R, Kiefer T, Brugger J. Sub micrometer ceramic structures fabricated by molding a polymer-derived ceramic. Microelectronic Engineering. 2012;97:272-5.

[7] Francis A. Progress in polymer-derived functional silicon-based ceramic composites for biomedical and engineering applications. Materials Research Express. 2018;5(6):062003.

[8] Arango-Ospina M, Xie F, Gonzalo-Juan I, Riedel R, Ionescu E, Boccaccini AR. Silicon oxycarbide based materials for biomedical applications. Applied Materials Today. 2020;18:100482.

[9] Duan WY, Yin XW, Ye F, Li Q, Han MK, Liu XF, et al. Synthesis and EMW absorbing properties of nano SiC modified PDC-SiOC. Journal of Materials Chemistry C. 2016;4(25):5962-9.

[10] Jia YJ, Ajayi TD, Roberts MA, Chung CC, Xu CY. Ultrahigh-temperature ceramic-polymer-derived SiOC ceramic composites for high-performance electromagnetic interference shielding. ACS Applied Materials & Interfaces. 2020;12(41):46254-66.

[11] Torrey JD. Polymer derived ceramic composites as environmental barrier coatings on steel, 2006, PhD thesis.

[12] Yang N, Gao M, Li J, Lu K. Nickel- containing magnetoceramics from water vapor- assisted pyrolysis of polysiloxane and nickel 2, 4- pentanedionate. Journal of the American Ceramic Society. 2020;103(1):145-57.

[13] Yang N, Lu K. Porous and ultrahigh surface area SiOC ceramics based on perhydropolysilazane and polysiloxane. Microporous and Mesoporous Materials. 2020:110477.

[14] Lu K, Li J. Fundamental understanding of water vapor effect on SiOC evolution during pyrolysis. Journal of the European Ceramic Society. 2016;36(3):411-22.

[15] Lu K, Erb D, Bawane K, Yang N. Comparison of traditional and flash pyrolysis of different carbon content silicon oxycarbides. Journal of the European Ceramic Society. 2019;39(10):3035-41.

[16] Colombo P. Polymer derived ceramics: From nano-structure to applications: DEStech Publications, Inc; 2010.

[17] Li JK, Lu K. Highly porous SiOC bulk ceramics with water vapor assisted pyrolysis. Journaal of the American Ceramic Society. 2015;98(8):2357-65.

[18] Li JK, Lu K, Lin TS, Shen FY. Preparation of micro-/mesoporous SiOC bulk ceramics. Journal of the American Ceramic Society. 2015;98(6):1753-61.

[19] Lu K. Porous and high surface area silicon oxycarbide-based materials-A review. Materials Science and Engineering R. 2015;97:23-49.

[20] Lu K, Erb D, Liu MY. Phase transformation, oxidation stability, and electrical conductivity of TiO_2-polysiloxane derived ceramics. Journal of Materials Science. 2016;51(22):10166-77.

[21] Lu K, Li JK. Fundamental understanding of water vapor effect on SiOC evolution during pyrolysis. Journal of the European Ceramic Society. 2016;36(3):411-22.

[22] Bawane K, Erb D, Lu K. Carbon content and pyrolysis atmosphere effects on phase development in SiOC systems. Journal of the European Ceramic Society. 2019;39(9):2846-54.

[23] Zheng JQ, Lu K. Electrically conductive and thermally stable SiC-TiC containing nanocomposites via flash pyrolysis. Journal of the American Ceramic Society. 2021;104(6):2460-71.

[24] Erb D, Lu K. Additive and pyrolysis atmosphere effects on polysiloxane-derived porous SiOC ceramics. Journal of the European Ceramic Society. 2017;37(15):4547-57.

[25] Saha A, Raj R, Williamson DL. A model for the nanodomains in polymer- derived SiCO. Journal of the American Ceramic Society. 2006;89(7):2188-95.

[26] Mera G, Tamayo A, Nguyen H, Sen S, Riedel R. Nanodomain structure of carbon- rich silicon carbonitride polymer- derived ceramics. Journal of the American Ceramic Society. 2010;93(4):1169-75.

[27] Lipowitz J, Rabe JA, Frevel LK, Miller RL. Characterization of nanoporosity in polymer-derived ceramic fibres by X-ray scattering techniques. Journal of Materials Science. 1990;25(4):2118-24.

[28] Sorarù GD, Modena S, Guadagnino E, Colombo P, Egan J, Pantano C. Chemical durability of silicon oxycarbide glasses. Journal of the American Ceramic Society. 2002;85(6):1529-36.

[29] Anand R, Sahoo SP, Nayak BB, Behera SK. Phase evolution, nanostructure, and oxidation resistance of polymer derived SiTiOC ceramic hybrid. Ceramics International. 2019;45(5):6570-6.

[30] Erb D, Lu K. Synthesis of SiOC using solvent-modified polymer precursors. Materials Chemistry and Physics. 2019;237:121844.

[31] Sharma A, Hesterberg D. 9 - Synchrotron radiation-based spatial methods in environmental biogeochemistry. In: Duarte RMBO, Duarte AC, editors. Multidimensional Analytical Techniques in Environmental Research: Elsevier; 2020. p. 231-65.

[32] Liao N, Xue W, Zhang M. Effect of carbon content on structural and mechanical properties of SiCN by atomistic simulations. Journal of the European Ceramic Society. 2012;32(6):1275-81.

[33] Amkreutz M, Frauenheim T. Understanding precursor-derived amorphous Si-C-N ceramics on the atomic scale. Physical Review B. 2002;65(13):134113.

[34] Resta N, Kohler C, Trebin H-R. Molecular dynamics simulations of amorphous Si–C–N ceramics: Composition dependence of the atomic structure. Journal of the American Ceramic Society. 2003;86(8):1409-14.

[35] Tomar V, Gan M, Kim H. Atomistic analyses of the effect of temperature and morphology on mechanical strength of Si-C-N and Si-C-O nanocomposites. Journal of the European Ceramic Society. 2010;30:2223-37.

[36] Matsunaga K, Iwamoto Y, Fisher CA, Matsubara H. Molecular dynamics study of atomic structures in amorphous Si-C-N ceramics. Journal of the Ceramic Society of Japan. 1999;107(1251):1025-31.

[37] Tersoff J. Modeling solid-state chemistry: Interatomic potentials for multicomponent systems. Physical Review B. 1989;39(8):5566.

[38] Resta N, Kohler C, Trebin HR. Molecular dynamics simulations of amorphous Si–C–N ceramics: composition dependence of the atomic structure. Journal of the American Ceramic Society. 2003;86(8):1409-14.

[39] Zhang M, Liao NB, Xue W, Yang P. Large-scale molecular dynamics modeling of boron-doped amorphous SiCO ceramics. Journal of Molecular Modeling. 2017;23(6):178.

[40] Zhang M, Liao N, Xue W, Yang P. Large-scale molecular dynamics modeling of boron-doped amorphous SiCO ceramics. Journal of Molecular Modeling. 2017;23(6):178.

[41] Senftle TP, Hong S, Islam MM, Kylasa SB, Zheng Y, Shin YK, et al. The ReaxFF reactive force-field: development, applications and future directions. npj Computational Materials. 2016;2(1):15011.

[42] Newsome DA, Sengupta D, Foroutan H, Russo MF, van Duin ACT. Oxidation of silicon carbide by O_2 and H_2O: A ReaxFF reactive molecular dynamics study, Part I. The Journal of Physical Chemistry C. 2012;116(30):16111-21.

[43] van Duin ACT, Dasgupta S, Lorant F, Goddard WA. ReaxFF: A Reactive Force Field for hydrocarbons. The Journal of Physical Chemistry A. 2001;105(41):9396-409.

[44] Vashisth A, Khatri S, Hahn SH, Zhang WW, van Duin ACT, Naraghi M. Mechanical size effects of amorphous polymer-derived ceramics at the nanoscale: Experiments and ReaxFF simulations. Nanoscale. 2019;11(15):7447-56.

[45] Gao HF, Wang HJ, Zhao ZH, Niu M, Su L, Wei Y. Reactive dynamics simulation study on the pyrolysis of polymer precursors to generate amorphous silicon oxycarbide structures. Journal of Physical Chemistry C. 2018;122(10):5767-73.

[46] Ponomarev I, van Duin ACT, Kroll P. Reactive Force Field for simulations of the pyrolysis of polysiloxanes into silicon oxycarbide ceramics. Journal of Physical Chemistry C. 2019;123(27):16804-12.

[47] Chenoweth K, Cheung S, Van Duin ACT, Goddard WA, Kober EM. Simulations on the thermal decomposition of a poly(dimethylsiloxane) polymer using the ReaxFF Reactive Force Field. Journal of the American Chemical Society. 2005;127(19):7192-202.

[48] Li W, Fukunishi M, Morgan BJ, Borkiewicz OJ, Chapman KW, Pralong V, et al. A reversible phase transition for sodium insertion in anatase TiO_2. Chemistry of Materials. 2017;29(4):1836-44.

[49] Jung H, Allan PK, Hu Y-Y, Borkiewicz OJ, Wang X-L, Han W-Q, et al. Elucidation of the local and long-range structural changes that occur in germanium anodes in lithium-ion batteries. Chemistry of Materials. 2015;27(3):1031-41.

[50] Koketsu T, Ma J, Morgan BJ, Body M, Legein C, Dachraoui W, et al. Reversible magnesium and aluminium ions insertion in cation-deficient anatase TiO_2. Nature Materials. 2017;16(11):1142-8.

[51] Aktulga HM, Fogarty JC, Pandit SA, Grama AY. Parallel reactive molecular dynamics: Numerical methods and algorithmic techniques. Parallel Computing. 2012;38(4-5):245-59.

[52] Ren Y. High-energy synchrotron X-ray diffraction and its application to in situ structural phase-transition studies in complex sample environments. JOM. 2012;64(1):140-9.

[53] Singh SKD, Lu K. SiOC coatings on yttria stabilized zirconia microspheres using a fluidized bed coating process. Powder Technology. 2022;396:158-66.

[54] Rau AV, Knott K, Lu K. Porous SiOC/SiC ceramics via an active-filler-catalyzed polymer-derived method. Materials Chemistry Frontiers. 2021;5(17):6530-45.

[55] Yang N, Lu K. Effects of transition metals on the evolution of polymer-derived SiOC ceramics. Carbon. 2021;171:88-95.

[56] Erb D, Lu K. Effects of SiO_2-forming additive on polysiloxane derived SiOC ceramics. Microporous and Mesoporous Materials. 2018;266:75-82.

[57] Ma R, Lu K, Erb D. Effect of solvent in preparation of SiOC bulk ceramics. Materials Chemistry and Physics. 2018;218:140-6.

[58] Yang N, Lu K. Porous and ultrahigh surface area SiOC ceramics based on perhydropolysilazane and polysiloxane. Microporous and Mesoporous Materials. 2020;306:110477.

[59] Erb D, Lu K. Effect of additive structure and size on SiO_2 formation in polymer-derived SiOC ceramics. Journal of the American Ceramic Society. 2018;101(12):5378-88.

[60] Wen Q, Yu Z, Riedel R. The fate and role of in situ formed carbon in polymer-derived ceramics. Progress in Materials Science. 2020;109:100623.

[61] Wang LX, Lu K, Ma RX. Effects of different polymer precursors on the characteristics of SiOC bulk ceramics. Appl Phys A-Materials. 2019;125(6).

[62] Ma RX, Lu K, Erb D. Effect of solvent in preparation of SiOC bulk ceramics. Materials Chemistry and Physics. 2018;218:140-6.

[63] Liu XL, Xue JM, Ren FY, Ye F, Fan XM, Liu YS, et al. Enhanced microwave-absorption properties of polymer-derived SiC/SiOC composite ceramics modified by carbon nanowires. Ceramics International. 2020;46(13):20742-50.

[64] Mera G, Navrotsky A, Sen S, Kleebe HJ, Riedel R. Polymer-derived SiCN and SiOC ceramics - structure and energetics at the nanoscale. Journal of Materials Chemistry A. 2013;1(12):3826-36.

[65] Su Q, Inoue S, Ishimaru M, Gigax J, Wang T, Ding H, et al. Helium irradiation and implantation effects on the structure of amorphous silicon oxycarbide. Scientific Reports. 2017;7(1):3900.

[66] Ishimaru M, Bae I-T, Hirotsu Y, Matsumura S, Sickafus KE. Structural relaxation of amorphous silicon carbide. Physical Review Letters. 2002;89(5):055502.